International Journal of Heat and Mass Transfer 186 (2022) 122514

Contents lists available at ScienceDirect

International Journal of Heat and Mass Transfer

journal homepage: www.elsevier.com/locate/hmt

Hierarchical design of material microstructures with thermal insulation properties

Yongfeng Zheng[a,d], Zhuojia Fu[b], Yingjun Wang[a,*], Xiang Lu[c], Jinping Qu[a,c], Chuanzeng Zhang[d]

[a] National Engineering Research Center of Novel Equipment for Polymer Processing, Key Laboratory of Polymer Processing Engineering (South China University of Technology), Ministry of Education, Guangdong Provincial Key Laboratory of Technique and Equipment for Macromolecular Advanced Manufacturing, School of Mechanical and Automotive Engineering, South China University of Technology, Guangzhou 510641, China
[b] Center for Numerical Simulation Software in Engineering and Sciences, College of Mechanics and Materials, Hohai University, Nanjing 210098, China
[c] Hubei Key Laboratory of Material Chemistry and Service Failure, School of Chemistry and Chemical Engineering, Huazhong University of Science & Technology, Wuhan 430074, China
[d] Department of Civil Engineering, University of Siegen, D-57068 Siegen, Germany

ARTICLE INFO

Article history:
Received 8 November 2021
Revised 29 December 2021
Accepted 30 December 2021
Available online 10 January 2022

Keywords:
Hierarchical materials
Biphasic materials
Multi-objective optimization
Thermal insulation

ABSTRACT

Composite materials with multiple properties are important for a range of engineering applications. Hence, this study focuses on topological design of hierarchical materials with multiple performance in both thermal insulation and mechanics. First, a novel multi-objective optimization function is defined to find a solution from the Pareto frontier, where the weight coefficients can be adjusted adaptively, to keep all the individual objective functions and their sensitivities stabilized at the same level during the optimization. Second, a new design strategy is proposed to achieve the hierarchical designs of biphasic material microstructures, they are periodically arranged by the porous base materials that are known in advance and independent of topology optimization. Third, sensitivity information and algorithm implementation are given in detail, and the bi-directional evolutionary structural optimization method is adopted to iteratively update the micro-structural topologies, by combining with the homogenization method. Last, numerical examples are provided to illustrate the benefits of the proposed design method, such as high efficiency, implementation easiness, good connectivity and clear interface between adjacent phases, etc.

1. Introduction

Metamaterials usually possess special properties such as ultralow mass density, high-strength, lightweight, sound reduction, energy absorbing, vibration isolation, heat and electricity insulation, etc. [1–6]. Topology optimization has been demonstrated as a powerful design tool to obtain advanced structures and material microstructures with various properties and performances [7,8]. In the past three decades, many topology optimization methods have been developed, typically including the density-based methods [9–14] and boundary representation methods [15–22]. Among these methods, the bi-directional evolutionary structural optimization (BESO) [23] conducts topological iterations by gradually adding 'useful materials' and removing 'ineffective materials', in accordance with the natural law of survival of the fittest. BESO shows many advantages such as conceptual simplicity, high efficiency, implementation easiness, and convenience for integration with popular commercial software.

Since the pioneer work by Sigmund [24], many researches employed topology optimization methods to design periodic material microstructures with expected and extreme material properties. Zhou et.al achieved systematic investigations into the computational design of biphasic and multi-phase cellular materials with extreme transport properties [25,26]. The parametric level set method has also been applied to create a range of micro-structured metamaterials including auxetic materials [27,28] and multifunctional metamateials with both negative Poisson's ratio and negative/zero thermal expansion [29]. Isogeometric topology optimization method has also been applied to generate elastic metamaterials [30–32]. BESO method [33–35] has been applied to design metamaterials to obtain maximum stiffness, thermal conductivity, extremal electromagnetic permeability, and permittivity. Page [36] investigated the high conductive conduit materials, which are distributed within a heat-generating volume. Alberdi and Khandelwal [37] carried out bi-material topology optimization by combin-

* Corresponding author.
E-mail address: wangyj84@scut.edu.cn (Y. Wang).

https://doi.org/10.1016/j.ijheatmasstransfer.2021.122514
0017-9310/© 2022 Elsevier Ltd. All rights reserved.

ing viscoplastic and hyperelastic phases for maximizing energy dissipation. Hamdia et.al [38] applied deep neural network to model the behaviors of two-phase material, and achieved the design of flexoelectric nanostructures. Li et al. [39,40] designed cellular structures consisting of multiple patches of material microstructures, and mechanical metamaterials with the negative Poisson's ratio properties. Topology optimization method has also been applied to generate pentamode metamaterials [41,42], which are a new type of three-dimensional solids but able to mimic the fluid behaviors. Zheng et.al obtained many favourable metamaterials with isotropic and auxetic properties, under the framework of evolutionary methods [43–45]. Other types of metamaterials have also been designed using topology optimization methods, such as [46–49].

Although many interesting metamaterials and associate composite structures have recently been obtained by using topology optimization, there is still a strong demand for investigation of more advanced materials and structures. Particularly, the family of multifunctional lattice composite materials and structures plays an important role for a range of advanced applications [50,51], such as the aircrafts and biomedical scaffolds. The majority of the current works are focused on the simultaneous designs of materials and composites that are hierarchical multiscale structures, such as [40,45,52,53], while few researchers have studied the design of both the multifunctional metamaterials and their underlying base materials. Furthermore, the connectivity between different shapes of microstructures is difficult to be guaranteed during the optimization, making them difficult for manufacturing. Most multifunctional designs utilized the direct weighting method and manually adjusted the weighting coefficients [33,54,55], and the design results strongly depend on the randomness and experiences of selecting the weight coefficients, which may make multifunctional materials difficult to obtain in terms of the Pareto solutions, when there are property conflicts between different materials.

To address the abovementioned problems, this study focuses on the multifunctional design of material microstructures with two phases, such as thermal insulation with bulk modulus, thermal insulation with shear modulus, and thermal insulation with two moduli. First, a novel multi-objective function is defined, where the weight coefficients can be adjusted adaptively, to keep the sub-objective functions and their sensitivities always stabilize at the same level during the optimization, this will ensure the algorithm to find solutions close to the Pareto front. Second, the biphasic hierarchical materials to be optimized are periodically arranged by the selected porous base materials (PBMs), since different PBMs exhibit different performances in thermal insulation and mechanics. Base material library is given in advance, where the topological configurations and equivalent properties of all PBMs are known, so they are independent of topology optimization. This paper only considers five types of PBMs but without losing any generality. Third, sensitivities of the multi-objective function with respect to the design variables are derived, so that the standard optimality criteria algorithm can be used. With the BESO [23] and the homogenization method [56,57], many favourable hierarchical material microstructures with multiple properties can be obtained. Last, numerical examples are provided to demonstrate the advantages of the proposed method.

2. Homogenization theory and optimization formulation

2.1. Homogenization theory

Fig. 1 illustrates the topological design of hierarchical material microstructures, macroscale is not considered but only used to explain the design strategy of this study. Composite structure in mesoscale is periodically arranged by one or two PBMs, and it is to be optimized by adopting the techniques of topology optimization and homogenization. Base materials are provided in microscale, they can be expanded to many enough as design needed, and not limit to those exhibited in Fig. 1.

In the framework of density-based methods, the physical property of the discretized element is interpolated by using a power-law scheme, this scheme has been demonstrated not only to ensure the free distribution of multiple materials, but also to produce clear topologies [58,59]. The equivalent elastic modulus of the two-phase composite materials in mesoscale can be interpolated by

$$\mathbf{E}(x_a) = x_a^p \mathbf{E}^1 + (1 - x_a^p)\mathbf{E}^2 \tag{1}$$

x_a denotes the binary design variable (1 or $x_{\min}$), where $x_{\min} = 0.001$ is utilized to avoid the singularity of elemental stiffness matrix. $\mathbf{E}(x_a)$ is the elemental property of the two-phase composite materials related to element a. $\mathbf{E}^1$ and $\mathbf{E}^2$ are the effective properties of the considered base materials, respectively, and $\mathbf{E}^1 > \mathbf{E}^2$. p is the penalty factor and is taken as 3 in this study. For the design of single-phase hierarchical material, phase 2 is specifically voids with $\mathbf{E}^2 = 0$. When the periodic boundary conditions are applied, the finite element method can be used to calculate the displacement field, and the following elemental stiffness matrix should be obtained before the finite element analysis:

$$\mathbf{K}_1 = \sum_{a=1}^{N} \mathbf{K}_1^a = \sum_{a=1}^{N} \int_Y \mathbf{b}_1^T \mathbf{E}(x_i)\mathbf{b}_1 dY \tag{2}$$

$\mathbf{K}_1$ and $\mathbf{K}a$ 1 are the global stiffness matrix and elemental stiffness matrix in mesoscale, respectively, $\mathbf{b}_1$ is the strain-displacement matrix. If periodic unit-cells (PUCs) of the hierarchical materials are smaller enough than the geometric size of the considered structure, the homogenization method can give us a way to approximately evaluate their properties [56]:

$$\mathbf{E}^H = \frac{1}{|Y|} \sum_{a=1}^{N} \int_Y \mathbf{E}(x_a)(\boldsymbol{\varepsilon}_0 - \boldsymbol{\varepsilon}) dY \tag{3}$$

Where $\mathbf{E}^H$ is the homogenized properties of the composite materials. Y denotes the area of the 2D unit cell, N is the elemental number to be discretized. $\boldsymbol{\varepsilon}_0$ and $\boldsymbol{\varepsilon}$ are the unit test strain field and the induced strain field, respectively. In 2D scenario, there are three kinds of initial unit test strains $\{1, 0, 0\}^T$, $\{0, 1, 0\}^T$ and $\{0, 0, 1\}^T$ along the x-, y- and shear-directions, if they are imposed on the PUC [57], we obtain

$$\mathbf{K}_1 \mathbf{u} = \sum_{a=1}^{N} \int_Y \mathbf{b}^T \mathbf{E}(x_a) dY \tag{4}$$

in which the right-hand side signifies the external forces induced by the three uniform strain fields, $\mathbf{u}$ is the unknown displacement field to be solved.

Similarly, the thermal conductivity of the a-th element with two phases can be interpolated as

$$\mathbf{k}(x_a) = x_a^p \mathbf{k}^1 + (1 - x_a^p)\mathbf{k}^2 \tag{5}$$

where $\mathbf{k}(x_a)$ is the interpolated conductivity of the a-th element in mesoscale. $\mathbf{k}^1$ and $\mathbf{k}^2$ are the thermal conductivities of the strong base material and weak base material, respectively, and $\mathbf{k}^1 > \mathbf{k}^2$. Other parameter settings are consistent with those expressed in Eq. (1). For the design of single-phase hierarchical material, phase 2 is specifically voids with $\mathbf{k}^2 = 0$. When the periodic boundary conditions are applied, the FEM can be used to calculate the temperature field, and the elemental temperature matrix should be obtained before the finite element analysis:

$$\mathbf{K}_2 = \sum_{a=1}^{N} \mathbf{K}_2^a = \sum_{a=1}^{N} \int_Y \mathbf{b}_2^T \mathbf{k}(x_a)\mathbf{b}_2 dY \tag{6}$$

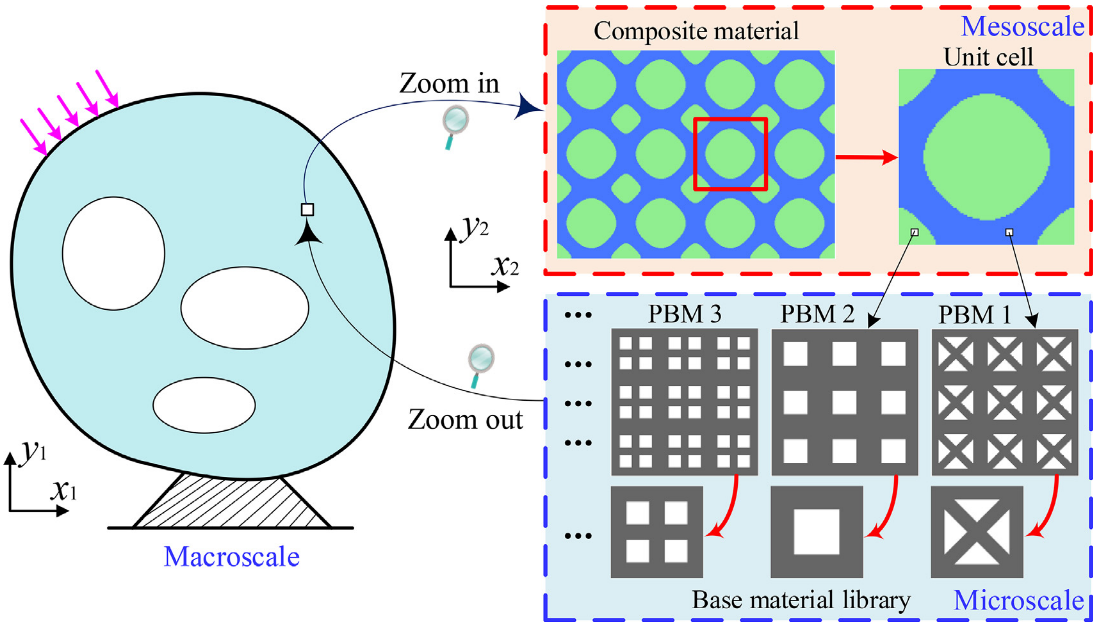

Fig. 1. Illustration for the topological design of hierarchical material microstructures.

$\mathbf{K}_2$ and **K**a 2 are the global stiffness matrix and elemental stiffness matrix in mesoscale, respectively, $\mathbf{b}_2$ is the strain-temperature matrix. According to the homogenization method, the equivalent thermal conductivity can be evaluated as

$$\mathbf{k}^H = \frac{1}{|Y|}\sum_{a=1}^{N}\int_Y \mathbf{k}(x_a)(\boldsymbol{\chi}_0 - \boldsymbol{\chi})dY \tag{7}$$

$\mathbf{k}^H$ is the homogenized thermal conductivity tensor, $\boldsymbol{\chi}_0$ and $\boldsymbol{\chi}$ are the unit temperature gradient field and the induced temperature gradient field, respectively. In 2D scenario, there are two uniform temperature gradient fields $\{1, 0\}^T$ and $\{0, 1\}^T$ along the x- and y-directions, if they are imposed on the PUC, we can obtain

$$\mathbf{K}_2\mathbf{t} = \sum_{a=1}^{N}\int_Y \mathbf{b}_2^T\mathbf{k}(x_i)dY \tag{8}$$

in which the right-hand side signifies the external temperatures induced by the two uniform strain fields, $\mathbf{t}$ is the unknown temperature field to be solved.

2.2. Optimization formulation

This study aims to seek for the hierarchical materials with optimized properties in both the thermal insulation and mechanics. Based on the BESO method, the corresponding multi-objective topology optimization formulation can be defined as

$$\begin{aligned}
&\text{Maximize}: g = \omega_1 f_1 + \omega_2 f_2\\
&\text{Subject to}: \ \mathbf{K}_1\mathbf{U}^{vi} = \mathbf{F}_1^{vi}\\
&\qquad\qquad \mathbf{K}_2\mathbf{T}^{vi} = \mathbf{F}_2^{vi}\\
&\qquad\qquad \sum_{a=1}^{N} x_a V_a \le V^*\\
&\qquad\qquad x_a = x_{\min} \text{ or } 1
\end{aligned} \tag{9}$$

where g is the multi-objective performance of the composite materials, f_1 and f_2 denote the single performance in mechanics and thermal insulation, ω_1 and ω_1 are the weighting coefficients imposed on the two performances in mechanics and thermal insulation, $\mathbf{K}_1$ and $\mathbf{K}_2$ are the global stiffness matrix and global temperature matrix of the design domain, $\mathbf{U}^{vi}$ and **F*vi* 1** are the global displacement vector and the external force vector induced by the mechanical test case, $\mathbf{T}^{vi}$ and **F*vi* 2** are the global temperature vector and the external force vector induced by the thermal test case, N is the total element number, x_a is the elemental density with binary value ($x_{\min}$ or 1), $x_{\min}$ is a small number used to avoid the computational singularity of $\mathbf{U}^{vi}$ and $\mathbf{T}^{vi}$. Also, V_a signifies the elemental volume, V^* denotes the specified material usages. It is noting that the parameters defined above are dimensionless for simplification. Next, we propose a novel weighting coefficients adjustment strategy, which is expressed as

$$\begin{cases}\omega_1 = \frac{1}{f_1^{old}}\\ \omega_2 = \frac{1}{f_2^{old}}\end{cases} \tag{10}$$

f_1^{old} and f_2^{old} are the sub-objective function values in the previous iteration, respectively. As the numerical algorithm proceeds, it is easy to find that weight coefficients will change constantly along with the changing of f_1^{old} and f_2^{old}. In this regard, the adjustment scheme can be deemed as an adaptive one. Additionally, this method can eliminate the difference in the magnitude order between the sub-objective function values, which is very likely to induce the ill-condition appearance of loads in multi-objective optimization. By normalizing each sub-objective function value in real time, the Pareto optimal solutions can be obtained easily. It is noting that weight coefficients are always known during topology optimization, because the sub-objective function values in the previous iteration have been already calculated. For the first iteration, the sub-objective function values of the initial design can be used to calculate f_1^{old} and f_2^{old}.

In 2D scenario, the homogenized elasticity modulus *EH ij* and thermal conductivity tensor *kH st* of composite materials are matrices with sizes of 3×3 and 2×2, respectively. This study mainly focuses on the maximum performances in thermal insulation and bulk modulus, thermal insulation and shear modulus, thermal insulation as well as bulk and shear moduli, the corresponding objective functions can be sequentially defined as

$$\begin{cases}g_1 = \frac{E_{11}+E_{22}+E_{12}+E_{21}}{f_1^{old}} + \frac{1}{f_2^{old}(k_{11}+k_{22})}\\ g_2 = \frac{E_{33}}{f_1^{old}} + \frac{1}{f_2^{old}(k_{11}+k_{22})}\\ g_3 = \frac{E_{11}+E_{22}+E_{12}+E_{21}+E_{33}}{f_1^{old}} + \frac{1}{f_2^{old}(k_{11}+k_{22})}\end{cases} \tag{11}$$

where E_{11} and E_{22} are the elastic coefficients along the x- and y-directions, respectively. E_{12} and E_{21} are the elastic coupling coef-

Fig. 2. Microstructures with different properties but have the same topological configurations and porosities.

ficients between the x- and y-directions, respectively, E_{33} corresponds to the elastic coefficient along the shear direction, k_{11} and k_{22} are heat transfer tensors along the x- and y-directions, respectively. Usually, the conductivities k_{12} and k_{21} along the coupling directions are much smaller than the values of k_{11} and k_{22}, so they are ignored in this study. Reciprocal of the summation of k_{11} and k_{22} are used in Eq. (11), because this study considers the maximum performance in thermal insulation, rather than the heat conduction.

3. Base material descriptions

This study evaluates the mesoscopic equivalent properties of five PBMs with arbitrary densities (between 0 and 1) by the homogenization method, it is noting that all the considered microstructures are generated, meshed and computed in Matlab software. As shown in Fig. 2, since different material properties can be induced by the same topological configurations and porosities, this study keeps the five micro-configurations unchanged, and try to ensure the same structural dimensions in themselves, so as to do fair comparisons. Fig. 3 gives the normalized elastic properties of the five PBMs, including their tensile coefficients, shear coefficients, Poisson's ratios in the x- and y-directions, and thermal conductivities in the x- and y-directions. In Fig. 3, E_s, ν_s, G_s and k_s are the elastic modulus, Poisson's ratio, shear modulus and thermal conductivity of the solid unit-cells, respectively. E_{11} and E_{22} are the elastic coefficients in the x- and y- directions, respectively. G denotes the shear modulus of the porous microstructures. ν_x and ν_y are the Poisson's ratios in the x- and y-directions, respectively. k_{11} and k_{22} are the thermal conductivities in the x- and y-directions, respectively.

As illustrated in Fig. 3, the A1 and A2 configurations show opposite Poisson's ratios and thermal conductivities in the x- and y-directions, but their elastic coupling and shear properties are always same for different densities. Curve trends in the A3 configuration are very close to those in the B configuration, implying that the two configurations have the similar performances in mechanics and heat conduction. Curves in the A4 configuration are completely different from other four configurations, where the Poisson's ratio does not change much when the density lies between 0.25 and 1.00. Furthermore, the tensile and shear performances of A4 are quite similar when the density ranges from 0 to 1.

To guide the potential readers, this study constructs fitting functions according to the physical quantities shown in Fig. 3, so as to easily obtain the mesoscopic equivalent properties with continuous densities between 0 and 1, which are given in Table 1. Based on these fitting functions, the mesoscopic effective properties related to a prescribed density can be directly obtained without re-applying the homogenization method. In addition, the least-squares method in mathematics is utilized to evaluate how well the constructed functions fit the real situations. The fitness value $R^2 = 1$ indicates that the given function perfectly fits the samples, whereas $R^2 = 0$ means that these given functions do not fit the samples at all. It is noting that 20 uniform density samples between 0.05 and 1 are selected to fit each function. As listed in Table 1, most fitting functions can achieve an accuracy of more than 99% by the polynomials with different orders, except for the Poisson's ratio function of 97.14% in A4 configuration, due to its poor continuity in Fig. 3. These R^2 values illustrate that these fitting functions are very close to the real situations.

Particularly, Table 2 lists five microstructures to constitute the composite materials with the same porosity to make fair comparisons, including the periodic unit-cells (PUCs), 3 × 3 periodic arrangements, effective elasticity matrixes and thermal conductivity matrixes. Table 3 lists their mechanical moduli and thermal conductivities of these five configurations. All the numerical results listed in Tables 2 and 3 are calculated based on the unit elastic modulus and unit thermal conductivity, and the Poisson's ratios in all PBMs are equal to 0.3.

As shown in Tables 2 and 3, although the topological configurations of five microstructures are symmetrical in both the x- and y-directions, they exhibit completely different performances in mechanics and thermal insulation. A1 configuration distributes more materials in x-direction than the ones in y-direction, while A2 configuration is the opposite. A3∼A5 configurations allocate the same amount of material usages in both the x- and the y-directions. Hence, A1 and A2 configurations are anisotropic in both the mechanics and heat transport, A3∼A5 configurations are orthotropic in mechanics but isotropic in heat transport. Although A1 and A2 materials with large thermal anisotropies can be widely used to guide the heat flow in a specific direction [60], their thermal homogeneities are usually very poor. Therefore, designers should choose the required material microstructures according to their actual applications such as heat guide, thermal insulation, and thermoelectrics, etc.

A1 and A2 configurations have the best tensile resistances and thermal conduction tensors in x- and y-directions, respectively. In addition, they possess the worst shear moduli, the middle bulk moduli and conductivities. A3∼A5 configurations have the same mechanical and thermal performances in both the x- and y-directions, the coupling tensors are equal to each other in xy- and yx-directions. A3 has the middle shear modulus, whereas its bulk modulus and conductivity are the best. A4 has the best shear modulus, the worst bulk modulus and conductivity. A5 has the middle bulk modulus, middle shear modulus and conductivity. It is interesting to find that the strength order in thermal conductivities are consistent with their bulk moduli, but has nothing to do with the shear moduli.

4. Sensitivity analysis and algorithm implementation

4.1. Sensitivity analysis

Topology optimization is a numerical solution technique, so sensitivity information related to objective function should be obtained to iteratively perform the calculation. For the design of single-phase porous material, the derivative of each homogenized mechanical and thermal tensor related to design variable x_a should

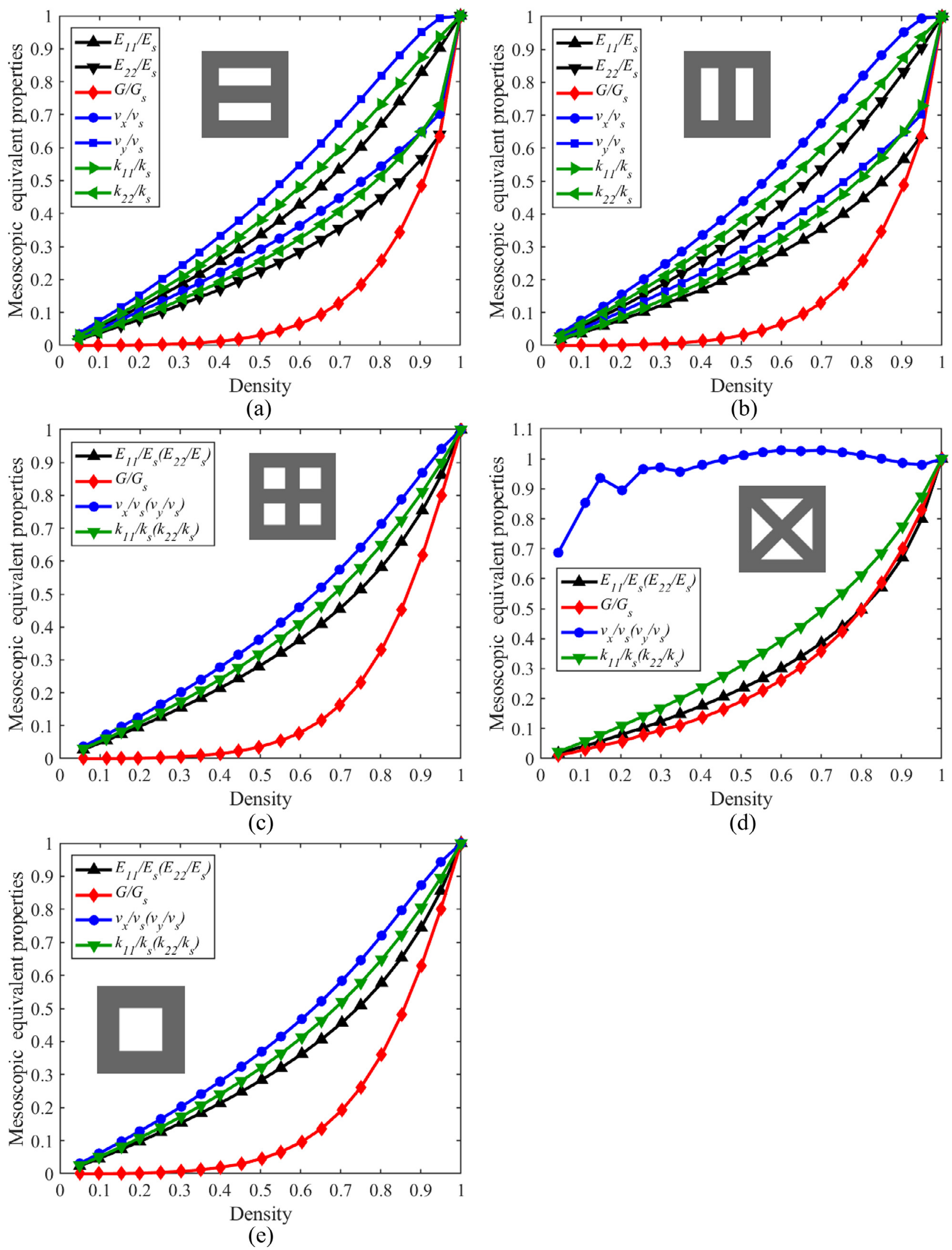

Fig. 3. Normalized effective elasticity matrix and thermal conductivity matrix of the considered microstructures. (a) A1 configuration; (b) A2 configuration; (c) A3 configuration; (d) A4 configuration; (e) A5 configuration.

Table 1
Fitting functions for the mesoscopic equivalent properties versus the PUC densities.

PUC	Normalized property	Fitting function	Fitness (R^2)
A1	E_{11} / E_s	$-0.8046\times^5 + 2.172\times^4 - 1.581\times^3 + 0.7454\times^2 + 0.4644x + 0.0032$	99.99%
	E_{22} / E_s	$20.2\times^5 - 46.57\times^4 + 38.83\times^3 - 13.8\times^2 + 2.385x - 0.0837$	99.09%
	v_x / v_s	$16.82\times^5 - 39.4\times^4 + 33.24\times^3 - 11.85\times^2 + 2.23x - 0.0723$	99.36%
	v_y / v_s	$-5.376\times^5 + 11.7\times^4 - 8.902\times^3 + 3.283\times^2 + 0.2841x + 0.0182$	99.99%
	G / G_s	$13.28\times^5 - 28.37\times^4 + 23.01\times^3 - 8.035\times^2 + 1.147x - 0.0471$	99.77%
	k_{11} / k_s	$-1.567\times^5 + 3.449\times^4 - 2.474\times^3 + 1.118\times^2 + 0.4701x + 0.0053$	99.99%
	k_{22} / k_s	$13.18\times^5 - 30.17\times^4 + 25.16\times^3 - 8.843\times^2 + 1.708x - 0.0542$	99.68%
A2	E_{11} / E_s	$20.2\times^5 - 46.57\times^4 + 38.83\times^3 - 13.8\times^2 + 2.385x - 0.0837$	99.09%
	E_{22} / E_s	$-0.8046\times^5 + 2.172\times^4 - 1.581\times^3 + 0.7454\times^2 + 0.4644x + 0.0032$	99.99%
	v_x / v_s	$-5.376\times^5 + 11.7\times^4 - 8.902\times^3 + 3.283\times^2 + 0.2841x + 0.0182$	99.99%
	v_y / v_s	$16.82\times^5 - 39.4\times^4 + 33.24\times^3 - 11.85\times^2 + 2.23x - 0.0723$	99.36%
	G / G_s	$13.28\times^5 - 28.37\times^4 + 23.01\times^3 - 8.035\times^2 + 1.147x - 0.0471$	99.77%
	k_{11} / k_s	$13.18\times^5 - 30.17\times^4 + 25.16\times^3 - 8.843\times^2 + 1.708x - 0.0542$	99.68%
	k_{22} / k_s	$-1.567\times^5 + 3.449\times^4 - 2.474\times^3 + 1.118\times^2 + 0.4701x + 0.0053$	99.99%
A3	E_{11} / E_s, E_{22} / E_s	$1.309\times^3 - 1.171\times^2 + 0.8743x - 0.0326$	99.88%
	v_x / v_s, v_y / v_s	$0.2279\times^3 + 0.2348\times^2 + 0.5447x + 0.0066$	99.97%
	G / G_s	$3.189\times^3 - 3.016\times^2 + 0.881x - 0.0645$	99.83%
	k_{11} / k_s, k_{22} / k_s	$0.6926\times^3 - 0.3423\times^2 + 0.6565x - 0.0115$	99.99%
A4	E_{11} / E_s, E_{22} / E_s	$13.56\times^6 - 35.54\times^5 + 36.35\times^4 - 17.69\times^3 + 4.379\times^2 - 0.0794x + 0.0144$	99.99%
	v_x / v_s, v_y / v_s	$-16.26\times^6 + 66.21\times^5 - 103.4\times^4 + 78.49\times^3 - 30.53\times^2 + 5.999x + 0.4755$	97.14%
	G / G_s	$3.266\times^6 - 7.895\times^5 + 8.049\times^4 - 3.466\times^3 + 0.8275\times^2 + 0.2196x - 0.0012$	99.99%
	k_{11} / k_s, k_{22} / k_s	$2.49\times^6 - 5.786\times^5 + 5.542\times^4 - 2.428\times^3 + 0.7349\times^2 + 0.4452x - 0.0017$	99.99%
A5	E_{11} / E_s, E_{22} / E_s	$1.332\times^3 - 1.193\times^2 + 0.8695x - 0.0299$	99.88%
	v_x / v_s, v_y / v_s	$0.1888\times^3 + 0.2956\times^2 + 0.5257x + 0.008$	99.95%
	G / G_s	$2.785\times^3 - 2.41\times^2 + 0.6599x - 0.0435$	99.90%
	k_{11} / k_s, k_{22} / k_s	$0.7015\times^3 - 0.3472\times^2 + 0.6512x - 0.0102$	99.99%

Table 2
Five microstructures considered in this study.

Type	Porosity	PUC	3 × 3 periodic arrangements	Effective elasticity matrix	Thermal conductivity matrix
A1	0.76		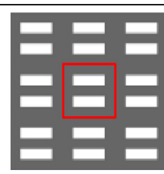	$\begin{bmatrix} 0.6738 & 0.1015 & 0 \\ 0.1015 & 0.4457 & 0 \\ 0 & 0 & 0.0749 \end{bmatrix}$	$\begin{bmatrix} 0.6749 & 0 \\ 0 & 0.4661 \end{bmatrix}$
A2	0.76		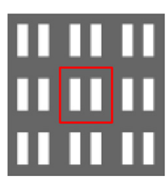	$\begin{bmatrix} 0.4457 & 0.1015 & 0 \\ 0.1015 & 0.6738 & 0 \\ 0 & 0 & 0.0749 \end{bmatrix}$	$\begin{bmatrix} 0.4661 & 0 \\ 0 & 0.6749 \end{bmatrix}$
A3	0.76		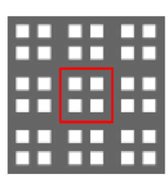	$\begin{bmatrix} 0.5811 & 0.1145 & 0 \\ 0.1145 & 0.5811 & 0 \\ 0 & 0 & 0.0969 \end{bmatrix}$	$\begin{bmatrix} 0.5946 & 0 \\ 0 & 0.5946 \end{bmatrix}$
A4	0.76		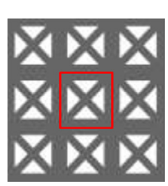	$\begin{bmatrix} 0.4921 & 0.1505 & 0 \\ 0.1505 & 0.4921 & 0 \\ 0 & 0 & 0.1670 \end{bmatrix}$	$\begin{bmatrix} 0.5602 & 0 \\ 0 & 0.5602 \end{bmatrix}$
A5	0.76		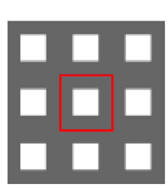	$\begin{bmatrix} 0.5759 & 0.1144 & 0 \\ 0.1144 & 0.5759 & 0 \\ 0 & 0 & 0.1081 \end{bmatrix}$	$\begin{bmatrix} 0.5928 & 0 \\ 0 & 0.5928 \end{bmatrix}$

Table 3
Equivalent elasticity moduli and thermal conductivities of A1∼A5 configurations.

Type	A1	A2	A3	A4	A5
Bulk modulus	1.3225	1.3225	1.3912	1.2852	1.3806
Shear modulus	0.0749	0.0749	0.0969	0.1670	0.1081
Conductivities	1.1410	1.1410	1.1892	1.1204	1.1856

be expressed as [33]

$$\begin{cases} \frac{\partial E_{ij}^H}{\partial x_a} = \frac{p x_a^{p-1}}{|Y|} \int_Y (\varepsilon_0 - \varepsilon)^T E_0 (\varepsilon_0 - \varepsilon) dY \\ \frac{\partial k_{st}^H}{\partial x_a} = \frac{p x_a^{p-1}}{|Y|} \int_Y (\chi_0 - \chi)^T k_0 (\chi_0 - \chi) dY \end{cases} \tag{12}$$

where *EH ij* and *kH st* denote an arbitrary tensor component in the mechanical and thermal property matrices, respectively, p is the penalty factor and equal to 3 in this study, x_a is the elemental density related to element a, ε_0 and ε are the unit test strain field and the induced strain field, respectively. χ_0 and χ are the unit temperature gradient field and the induced temperature gradient field, respectively. E_0 and k_0 are the mechanical and heat transport properties of base material, respectively. If the cellular materials are biphasic, the derivative of the homogenized tensor with respect to design variable can be calculated by [59,61]

$$\begin{cases} \frac{\partial E_{ij}^H}{\partial x_a} = \frac{p x_a^{p-1}}{|Y|} \int_Y (\varepsilon_0 - \varepsilon)^T \left(E_{ij}^1 - E_{ij}^2\right) (\varepsilon_0 - \varepsilon) dY \\ \frac{\partial k_{st}^H}{\partial x_a} = \frac{p x_a^{p-1}}{|Y|} \int_Y (\chi_0 - \chi)^T \left(k_{st}^1 - k_{st}^2\right) (\chi_0 - \chi) dY \end{cases} \tag{13}$$

where *E*1 *ij* and *E*2 *ij* are the equivalent elasticity moduli of strong material and weak material, respectively. *k*1 *st* and *k*2 *st* are the thermal conductivity moduli of strong material and weak material, respectively. This study considers three kinds of multi-objective performances including thermal insulation with bulk modulus, thermal insulation with shear modulus and thermal insulation with bulk and shear moduli, their respective sensitivity information can be mathematically derived as

$$\begin{cases} \frac{\partial g_1}{\partial x_a} = p x_a^{p-1} \left(\frac{1}{f_1^{old}} \sum_{i,j=1}^{2} \frac{\partial E_{ij}^H}{\partial x_a} - \frac{\frac{\partial k_{11}^H}{\partial x_a} + \frac{\partial k_{22}^H}{\partial x_a}}{f_2^{old} (k_{11} + k_{22})^2} \right) \\ \frac{\partial g_2}{\partial x_a} = p x_a^{p-1} \left(\frac{1}{f_1^{old}} \frac{\partial E_{33}^H}{\partial x_a} - \frac{\frac{\partial k_{11}^H}{\partial x_a} + \frac{\partial k_{22}^H}{\partial x_a}}{f_2^{old} (k_{11} + k_{22})^2} \right) \\ \frac{\partial g_3}{\partial x_a} = p x_a^{p-1} \left(\frac{1}{f_1^{old}} \left(\sum_{i,j=1}^{2} \frac{\partial E_{ij}^H}{\partial x_a} + \frac{\partial E_{33}^H}{\partial x_a} \right) - \frac{\frac{\partial k_{11}^H}{\partial x_a} + \frac{\partial k_{22}^H}{\partial x_a}}{f_2^{old} (k_{11} + k_{22})^2} \right) \end{cases} \tag{14}$$

where f_1^{old} and f_2^{old} are the sub-objective function values in the previous iteration, and they are known in the sensitivity analysis of this iteration.

To avoid the common numerical issues including checkerboard form and mesh-dependency, some necessary strategies should be applied during optimization. As a heuristic method, sensitivity filtering has been demonstrated as a simple but efficient way to stabilize the topology optimization algorithm, which is originally used in image processing [44,62]. It can eliminate the small structural features below a prescribed size in the topologies, such as:

$$\alpha_a = \frac{\sum_{a=1}^{N} \omega(r_{ab}) \alpha_b}{\sum_{a=1}^{N} \omega(r_{ab})} \tag{15}$$

α_a is the filtered sensitivity related to element a, α_b is the sensitivity information related to element b, whose position is close to element a, N is the total element number discretized in the design domain, a and b indicate the a-th and b-th element, respectively, r_{ab} is the central distance between element a and b, $\omega(r_{ab})$ is the weighting factor related to r_{ab}, which can be further defined as

$$\omega_{ab} = \begin{cases} r_{\min} - r_{ab}, & if\ r_{ab} < r_{\min} \\ 0, & if\ r_{ab} \geq r_{\min} \end{cases} \tag{16}$$

where $r_{\min}$ is the specified filter radius, big filter radius means more structural details will be filtered, and vice versa. In evolutionary optimization algorithm, according to the calculation experiences [57], $r_{\min}$ should be selected as 4–6 times of the size of one element to obtain favorable designs.

Although sensitivity filtering is used, the structural evolution may still be unstable and the structural topology may not converge very well. This phenomenon attributes to the inaccurate estimation of sensitivity numbers, especially for the boundary elements which are originally not involved in finite element analysis. In this respect, Huang and Xie proposed an averaging operation as follows [23]:

$$\bar{\alpha}_a = \eta_1 \alpha_a^k + \eta_2 \alpha_a^{k-1} \tag{17}$$

where $\bar{\alpha}_a$ is the averaged sensitivity related to element a, α_a^k and α_a^{k-1} are the filtered sensitivities related to element a in the k-th and (k-1)-th iteration, η_1 and η_2 are the weight coefficients applied to α_a^k and α_a^{k-1}, and the two are respectively taken as 0.3 and 0.7 in this study. It is easy to find that we focus more on the sensitivity information in the previous iteration, to further stabilize the multi-objective algorithm. Furthermore, negative sensitivities may occur in Eq. (14), which will make the optimality criteria method fail to work in topology optimization. Since topological evolution in the BESO method is individually depended on the sequence of the elemental sensitivities, and regardless of their numerical values. Hence, all sensitivities can be added with a same positive number to prevent the occurrence of negative values, at the same time, their sequences can be well maintained.

$$\widehat{\alpha}_a = \bar{\alpha}_a + \left|\bar{\alpha}_c^{\min}\right| \tag{18}$$

$\widehat{\alpha}_a$ is the final sensitivity information with respect to element a, which will be used to determine the elemental addition and deletion during evolution, $\bar{\alpha}_a$ is the averaged sensitivity related to element a, $\bar{\alpha}_c^{\min}$ is the minimum negative sensitivity related to element c. All sensitivities will be non-negative through the operation in Eq. (18).

4.2. Algorithm implementation

The algorithm flowchart of the evolutionary algorithm for the design of hierarchical material microstructures is shown in Fig. 4, where the red dotted box represents the topology optimization loop. A complete optimization loop includes matrices assembly in mechanics and heat transport, FEA at two performances, sensitivity calculation, filtering, averaging and modification, variables updating, etc. The blue dotted box produce the porous base materials, which includes the base material library creating, evaluate the properties of all base materials, determination of property fitting functions and select the candidate base materials as design needed. This process is independent of topology optimization, so the proposed algorithm is more efficient to obtain hierarchical material microstructures than the two-scale design methods.

In evolutionary method, the target volume for the next iteration should be given to determinate the amount of material removal, which can be expressed as

$$V_{k+1} = \begin{cases} V_k(1 - er), & if\ V_{k+1} > V^* \\ V^*, & if\ V_{k+1} \leq V^* \end{cases} \tag{19}$$

where V_k denotes the structural volume of the current iteration, V_{k+1} is the target volume of the next iteration, er is the evolutionary ratio, V^* refers to the specified material usage. If V^* is obtained,

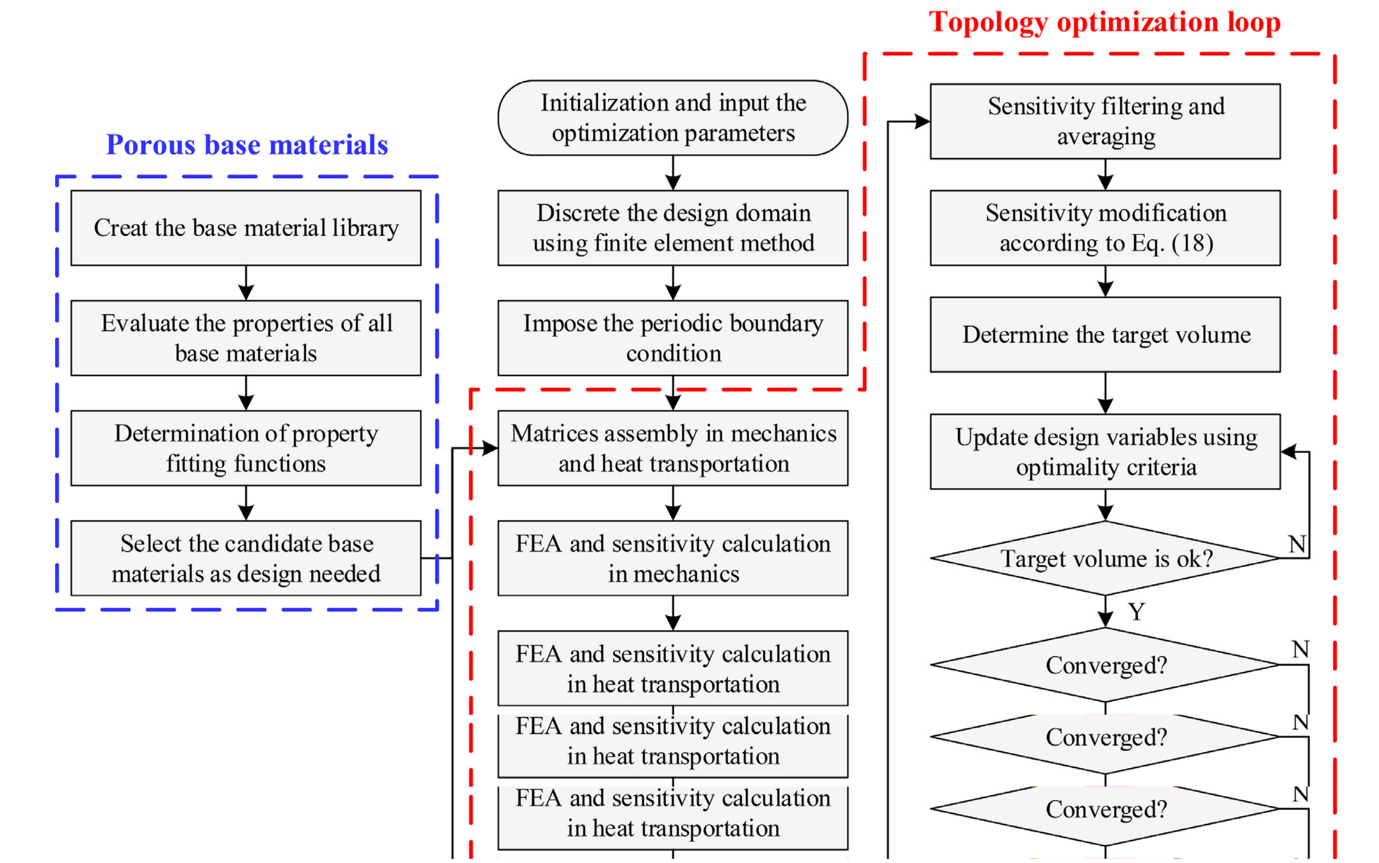

Fig. 4. Algorithm flowchart for the design of hierarchical materials.

satisfactory convergence accuracy should be given to terminate the evolutionary algorithm, such as

$$error = \left| \frac{\sum_{i=1}^{M} (g_{k-i+1} - g_{k-M-i+1})}{\sum_{i=1}^{M} g_{k-i+1}} \right| \leq \tau \tag{20}$$

where k is the current iteration number, $g_{k\text{-}i\,+\,1}$ and $g_{k-M\text{-}i\,+\,1}$ are the objective function values in the (k-i + 1)-th and (k-M-i + 1)-th iterations, respectively. $M = 5$ signifies that evolutionary algorithm obtains the final design after at least 10 consecutive iterations, so as to ensure favorable solutions. τ is the specified convergence accuracy, this study takes it as 0.001.

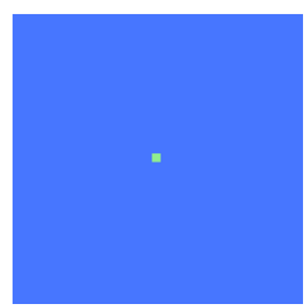

Fig. 5. Initial design.

5. Numerical examples

Using the PBMs provided in Table 2, this section shows four examples to obtain hierarchical material microstructures with different properties. The first one focuses on the design of single-performance composite materials, to maximize the bulk modulus, shear modulus and thermal insulation, the last three aim to obtain multifunctional performances in both the mechanics and thermal insulation. All numerical examples start from the same initial structure, as depicted in Fig. 5. A rectangular hole is inserted into the center of the design domain to simulate the optimization progress, due to the periodic boundary conditions imposed in the homogenization method. Although evolutionary algorithm can perform the elemental addition and deletion simultaneously, it is best to start with a near-full design to ensure all elements have chances to appear in each iteration. The discretized elements in all examples are 100 × 100, filter radius is set to 5 and evolutionary ratio is taken as 0.02. Table 4 lists eight cases to be analyzed, M1 and M2 indicate the strong material and weak material, which are represented by the blue color and green color, respectively. In the following numerical examples, all the homogenized tensors related to strong material M1 should be bigger enough than the weak material M2, so as to ensure stable optimizations, because M1 and M2 may possess multiple moduli due to their non-isotropic properties in both the mechanics and thermal insulation.

In case 1~4, M2 is the same one, whereas case 5~8 adopt the same M1. Additionally, all the numerical results are dimensionless for simplification. Moreover, MH is an indicator defined to express the compound performance of the obtained material microstructure, the bigger MH value the better compound performance, and vice versa. MH is calculated by Eq. (11) when both the weight coefficients are equal to 1. It should be noted that conductivities defined in the following tables refers to the summation of the thermal conductivities in both the x- and y-directions.

Table 4
Analysis cases.

Materials	Case 1	Case 2	Case 3	Case 4	Case 5	Case 6	Case 7	Case 8
M1	A1	A2	A3	A4	A5	A5	A5	A5
M2	A5	A5	A5	A5	A1	A2	A3	A4

Table 5
Bulk modulus maximization.

Type	Case 1	Case 2	Case 3	Case 4
PUC				
3 × 3 periodic arrangements	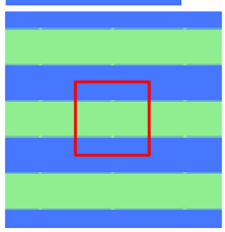	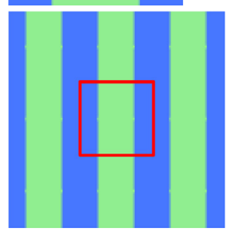	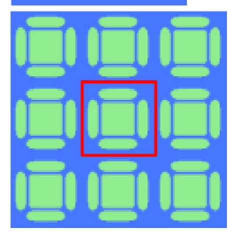	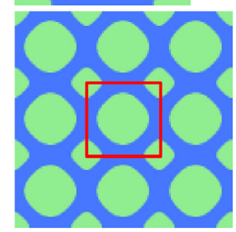
Equivalent elasticity matrix	$\begin{bmatrix} 1.2875 & 0.1715 & 0 \\ 0.1715 & 0.8046 & 0 \\ 0 & 0 & 0.1459 \end{bmatrix}$	$\begin{bmatrix} 0.8046 & 0.1715 & 0 \\ 0.1715 & 1.2875 & 0 \\ 0 & 0 & 0.1459 \end{bmatrix}$	$\begin{bmatrix} 1.0184 & 0.1833 & 0 \\ 0.1833 & 1.0184 & 0 \\ 0 & 0 & 0.1631 \end{bmatrix}$	$\begin{bmatrix} 0.9033 & 0.2401 & 0 \\ 0.2401 & 0.9033 & 0 \\ 0 & 0 & 0.2397 \end{bmatrix}$
Bulk modulus	2.4351	2.4351	2.4035	2.2868

Table 6
Shear modulus maximization.

Type	Case 1	Case 2	Case 3	Case 4
PUC				
3 × 3 periodic arrangements	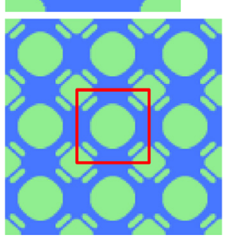	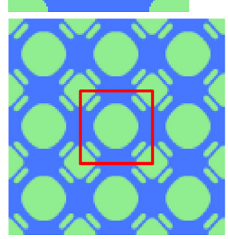	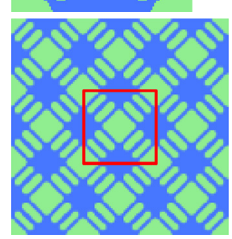	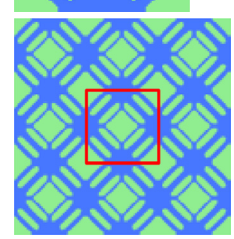
Equivalent elasticity matrix	$\begin{bmatrix} 0.9736 & 0.1959 & 0 \\ 0.1959 & 0.8397 & 0 \\ 0 & 0 & 0.1610 \end{bmatrix}$	$\begin{bmatrix} 0.8397 & 0.1959 & 0 \\ 0.1959 & 0.9736 & 0 \\ 0 & 0 & 0.1610 \end{bmatrix}$	$\begin{bmatrix} 0.9293 & 0.2173 & 0 \\ 0.2173 & 0.9293 & 0 \\ 0 & 0 & 0.1898 \end{bmatrix}$	$\begin{bmatrix} 0.8960 & 0.2488 & 0 \\ 0.2488 & 0.8960 & 0 \\ 0 & 0 & 0.2662 \end{bmatrix}$
Shear modulus	0.1610	0.1610	0.1898	0.2662

5.1. Design for single performance

This example aims to obtain some single-performance material microstructures, including the design of bulk modulus, shear modulus and thermal insulation. Both the elastic moduli and thermal conductivities in PBMs are set to 3 and 1, respectively. The specified material usages for M1 and M2 are the same value of 0.5, cases 1∼4 listed in Table 2 are analyzed to compare the micro-structural performances. Tables 5–7 list all the topological and numerical results pertaining to bulk modulus, shear modulus and thermal insulation, respectively. Specifically, insulation values listed in Table 7 are calculated by the reciprocal of the summation of k_{11} and k_{22}.

As listed in Table 5, the analyzed four cases exhibit completely different topologies, indicating different tensile resistances in A1∼A4 microstructures. Case 1 and case 2 show the bar-shaped configurations in the x- or y-directions, and they have the best bulk moduli among the four cases, which possess a little advantage over case 3. The final topology in case 3 is similar to the solid design, but case 4 is similar to the traditional shear modulus design, because the shear modulus in A4 microstructure is far better than its bulk modulus. Furthermore, case 3 and case 4 exhibit the

Table 7
Thermal insulation optimization.

Type	Case 1	Case 2	Case 3	Case 4
PUC			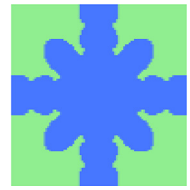	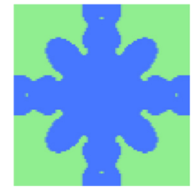
3 × 3 periodic arrangements	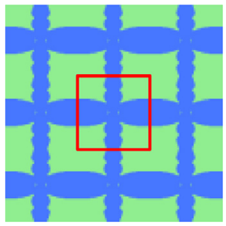	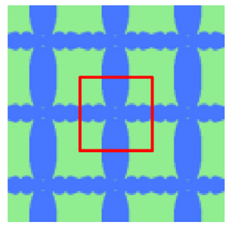	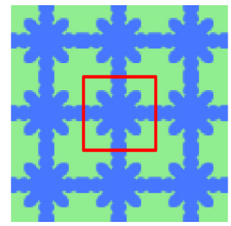	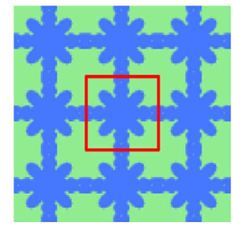
Thermal conductivity matrix	$\begin{bmatrix} 3.5145 & 0 \\ 0 & 2.3941 \end{bmatrix}$	$\begin{bmatrix} 2.3941 & 0 \\ 0 & 3.5145 \end{bmatrix}$	$\begin{bmatrix} 3.0254 & 0 \\ 0 & 3.0254 \end{bmatrix}$	$\begin{bmatrix} 2.8517 & 0 \\ 0 & 2.8517 \end{bmatrix}$
Insulation	0.1692	0.1692	0.1653	0.1753

same tensile resistances in both the x- or y-directions, respectively. Case 4 has the worst bulk modulus of 2.2868.

As listed in Table 6, four topologies converge to the octagon-shaped configurations, and there are same amount of material distributions in the x- and y-directions. Case 1 and case 2 have the same topologies, the topological configurations in case 3 and case 4 are also the same, which explains that the topological design in shear modulus is not easily affected by the constituted PBMs. Case 4 has a far-leading shear moduli of 0.2662 when compared to others, and the shear moduli in case 1 and case 2 are the worst ones of 0.1610.

As listed in Table 7, different cases converge to the same topologies, because they have the same amount of connected domains when small holes are ignored. M2 distributes in the four corners of the design domain to separate two PBMs strictly, even though M1 in all cases are well connected, the reason for this phenomenon is that M2 has smaller conductivity than M1. Case 1 distributes more materials in the x-direction, whereas cases 2 appears more materials in the y-direction. Cases 3 and case 4 have the same amount of material distributions in both the x- and y-directions, respectively. Case 4 has the best insulation performance, and case 3 is the worst one to insulate the heat conduction.

5.2. Thermal insulation and bulk modulus optimization

This example aims to obtain multifunctional materials with favorable tensile resistance and thermal insulation, eight cases listed in Table 4 are used to illustrate the composite properties of material microstructures. For all cases, the elastic moduli of two PBMs to make up M1 and M2 are equal to 10 and 1, respectively, the thermal conductivity settings for both base materials are also the same. In this regard, M1 has the better mechanics but worse insulation performances simultaneously, whereas M2 possesses the opposite performances, this example illustrates how the conflict topologies will be. Table 8 lists the PUCs, 3 × 3 periodic arrangements and all the numerical results under soft A5, Table 9 lists all the topological and numerical results under hard A5, Fig 0.6 depicts the evolutionary histories related to case 1 and case 5.

As listed in Table 8, case 1 and case 2 show the dumbbell-shaped topological configurations in x- or y-directions, respectively. Case 3 and case 4 exhibit the similar fan-shaped configurations. All the equivalent elasticity matrixes are orthotropic, thermal conductivity matrixes in the previous two cases are anisotropic, and the latter two are isotropic. Although case 1 and case 2 possess the minimum thermal conductivities corresponding to the best insulation performance, their bulk moduli and MHs are the worst ones among the four cases. Case 3 has the worst insulation performance, its bulk modulus and MH are the middle ones. Case 4 possesses the best bulk modulus and middle conductivity, and its MH value is the highest one, signifying that case 4 performs the best compound performances. The strength order of the composite performances in thermal insulation and bulk modulus, is consistent with the sequence of their bulk moduli, and has nothing to do with the thermal conductivities.

As listed in Table 9, case 5 and case 6 show the dumbbell-shaped topological configurations in y- or x-directions, respectively, both of them are opposite to those obtained in case 1 and case 2, which means that the interchange of M1 and M2 has a great impact on the design of composite material microstructures. Case 7 and case 8 exhibit the fan-shaped configurations at the same time, which are consistent with case 3 and case 4, this situation tells us that if the considered microstructures are symmetrical along the 45° diagonal, the obtained topologies are most likely the same, in spite of their numerical results are different. Four equivalent elasticity matrixes are orthotropic, thermal conductivity matrixes are anisotropic in case 5 and case 6, and isotropic in case 7 and case 8. The previous two cases possess the best insulation performance due to the minimum conductivities, but their bulk moduli and MHs are the lowest one. Case 7 has the best bulk modulus and MH value, its conductivity is 6.1626, which has a little advantage over that of case 8. The bulk modulus and conductivity in case 8 are the middle ones, leading to the middle MH value of 4.3348. The strength order of the four compound performances also corresponds to the sequence of their bulk moduli and conductivities. In addition, it is interesting to find that case 4 related to A4 microstructure performs the best MH value among cases 1∼4. However, case 7 related to A3 microstructure performs the best MH value among cases 5∼8. These facts show that experiences from single-phase designs are not effective for the biphasic designs.

As depicted in Fig. 6, the curves related to objective function, sub-objective function and volume fraction of case 1 and case 5 are stable enough, demonstrating that the evolutionary method has powerful ability to obtain the hierarchical material microstructures. The two curves of objective functions are basically equal to 2 during optimization, and the sub-objective functions always approach to 1, and they have no obvious shocks, which can be further

Table 8
Optimized thermal insulation and bulk modulus for soft A5.

Type	Case 1	Case 2	Case 3	Case 4
PUC	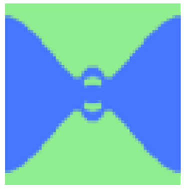	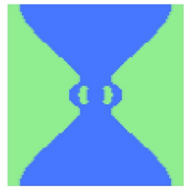		
3 × 3 periodic arrangements	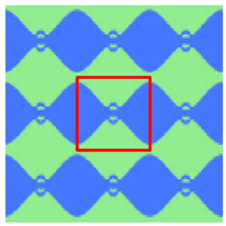	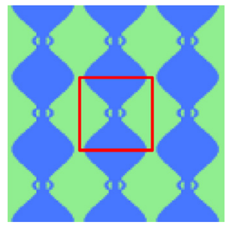	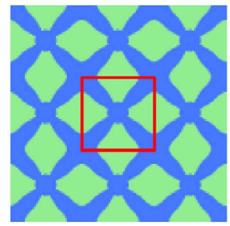	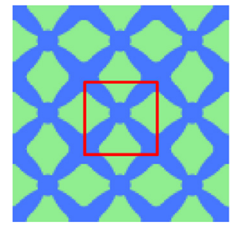
Equivalent elasticity matrix	$\begin{bmatrix} 2.1901 & 0.2392 & 0 \\ 0.2392 & 1.2443 & 0 \\ 0 & 0 & 0.2271 \end{bmatrix}$	$\begin{bmatrix} 1.2443 & 0.2392 & 0 \\ 0.2392 & 2.1901 & 0 \\ 0 & 0 & 0.2271 \end{bmatrix}$	$\begin{bmatrix} 1.5514 & 0.5510 & 0 \\ 0.5510 & 1.5514 & 0 \\ 0 & 0 & 0.4495 \end{bmatrix}$	$\begin{bmatrix} 1.6031 & 0.6567 & 0 \\ 0.6567 & 1.6031 & 0 \\ 0 & 0 & 0.6489 \end{bmatrix}$
Thermal conductivity matrix	$\begin{bmatrix} 3.4725 & 0 \\ 0 & 2.1879 \end{bmatrix}$	$\begin{bmatrix} 2.1879 & 0 \\ 0 & 3.4725 \end{bmatrix}$	$\begin{bmatrix} 3.0907 & 0 \\ 0 & 3.0907 \end{bmatrix}$	$\begin{bmatrix} 2.9193 & 0 \\ 0 & 2.9193 \end{bmatrix}$
Bulk modulus	3.9128	3.9128	4.2048	4.5192
Conductivities	5.6604	5.6604	6.1814	5.8386
MH	4.0895	4.0895	4.3666	4.6905

Table 9
Optimized thermal insulation and bulk modulus for hard A5.

Type	Case 5	Case 6	Case 7	Case 8
PUC	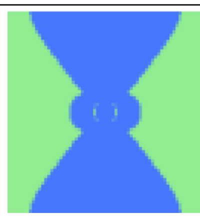	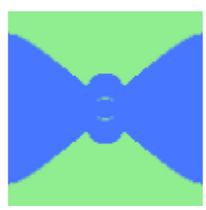		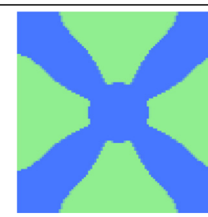
3 × 3 periodic arrangements	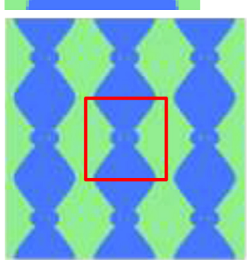	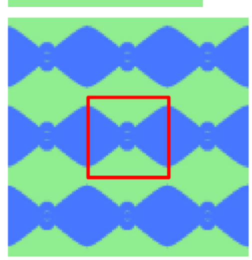	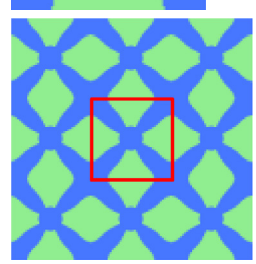	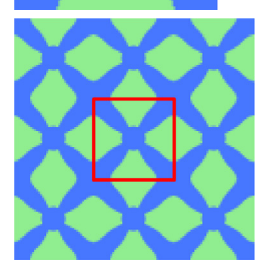
Equivalent elasticity matrix	$\begin{bmatrix} 1.3284 & 0.2257 & 0 \\ 0.2257 & 2.3003 & 0 \\ 0 & 0 & 0.1738 \end{bmatrix}$	$\begin{bmatrix} 2.3003 & 0.2257 & 0 \\ 0.2257 & 1.3284 & 0 \\ 0 & 0 & 0.1738 \end{bmatrix}$	$\begin{bmatrix} 1.5809 & 0.5699 & 0 \\ 0.5699 & 1.5809 & 0 \\ 0 & 0 & 0.4761 \end{bmatrix}$	$\begin{bmatrix} 1.4518 & 0.6340 & 0 \\ 0.6340 & 1.4518 & 0 \\ 0 & 0 & 0.5288 \end{bmatrix}$
Thermal conductivity matrix	$\begin{bmatrix} 2.8566 & 0 \\ 0 & 3.0932 \end{bmatrix}$	$\begin{bmatrix} 3.0932 & 0 \\ 0 & 2.8566 \end{bmatrix}$	$\begin{bmatrix} 3.0813 & 0 \\ 0 & 3.0813 \end{bmatrix}$	$\begin{bmatrix} 3.0630 & 0 \\ 0 & 3.0630 \end{bmatrix}$
Bulk modulus	4.0801	4.0801	4.3015	4.1716
Conductivities	5.9498	5.9498	6.1626	6.1260
MH	4.2482	4.2482	4.4638	4.3348

demonstrated by the topological evolutions shown in Fig. 6. Additionally, as the removal of inefficient materials, volume fractions gradually converge to the prescribed value of 0.5 in the 36th iteration, then the evolutionary algorithm needs about 10 iterations more to obtain the satisfactory accuracies.

5.3. Thermal insulation and shear modulus optimization

This example aims to obtain the composite materials with optimized thermal insulation and shear modulus, eight cases are utilized to analysis as explained in Sections 5.2. For all cases, the elastic moduli of two base materials to make up M1 and M2 are set to 3 and 1, respectively. The thermal conductivities of two base materials are equal to 5 and 1, respectively. Table 10 lists the PUCs, 3 × 3 periodic arrangements and all the numerical results under soft A5, Table 11 lists all the topological and numerical results under hard A5, Fig. 7 shows the evolutionary histories of case 4 and case 8.

As listed in Table 10, the topologies in case 1 and case 2 exhibit dumbbell-shaped configurations, little materials appear in the center of the design domain to reduce heat transfer, both of them have more materials distributed in the *x*- or *y*-direction, respec-

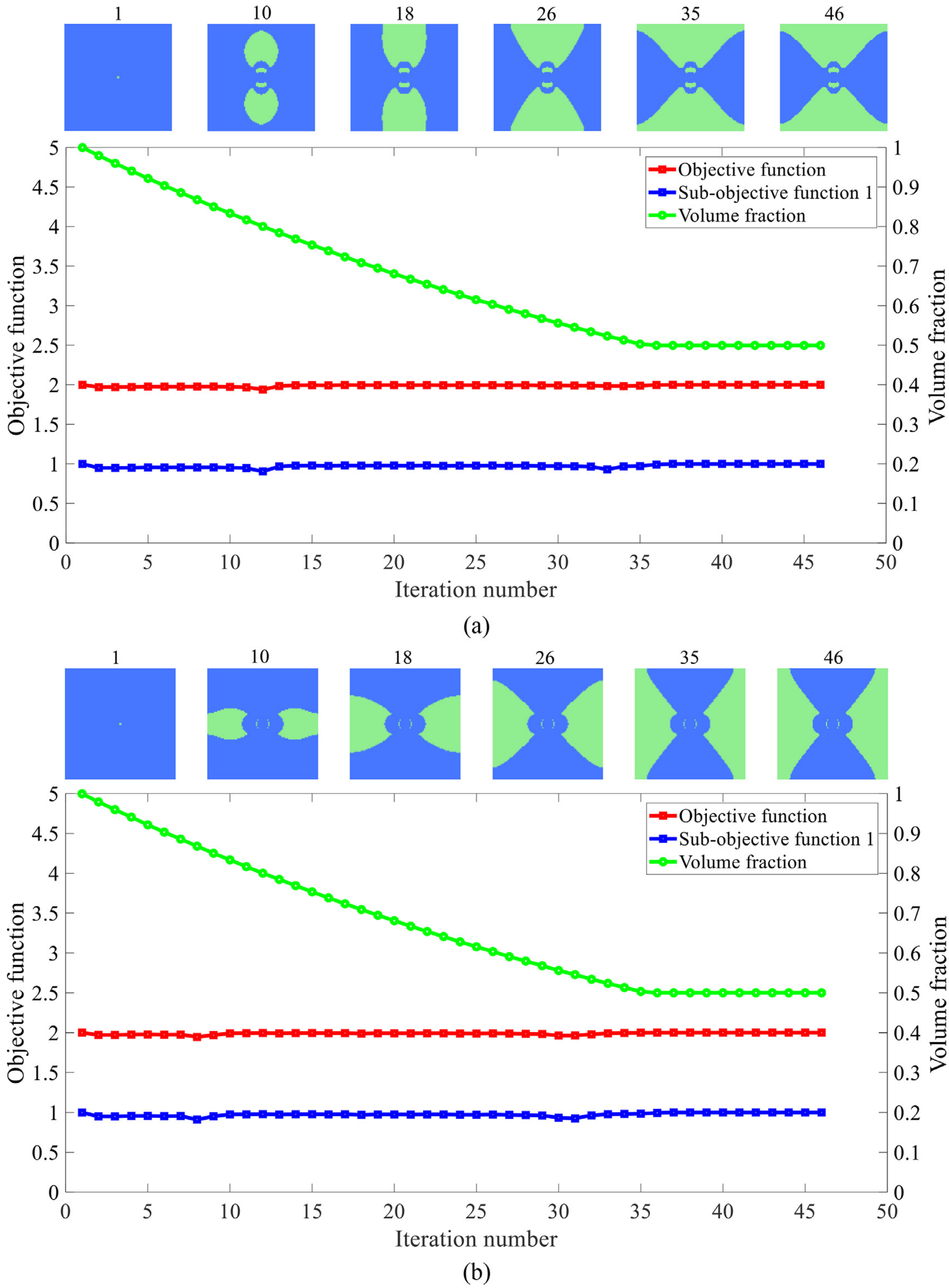

Fig. 6. Evolutionary histories of case 1 and case 5. (a) Soft A5 condition; (b) hard A5 condition.

tively, since their respective strong-phase materials A1 and A2 are also like this. Case 3 and case 4 converge to the same fan-shaped topologies. All the obtained equivalent elasticity matrixes are orthotropic, but the previous two thermal conductivity matrixes are anisotropic, the latter two are isotropic. Case 1 and case 2 possess the worst shear moduli and the best insulation performances, their MH values are the middle ones of 0.5013. Case 3 has the middle shear modulus and maximum conductivity, its compound performance in shear modulus and thermal insulation is the lowest one. Case 4 has a far-leading shear modulus and middle insulation value, and performs the best performance. The four compound performances have nothing to do with the magnitude of the shear moduli and conductivities.

As listed in Table 11, case 5 and case 6 exhibit the opposite dumbbell-shaped topological configurations in *y*- and *x*-directions, respectively. This situation illustrates that the interchange of M1 and M2 will seriously affect the hierarchical designs in shear modulus and thermal insulation. Case 7 and case 8 show the same fan-

Table 10
Optimized thermal insulation and shear modulus for soft A5.

Type	Case 1	Case 2	Case 3	Case 4
PUC	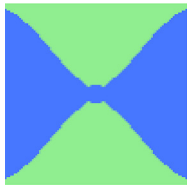	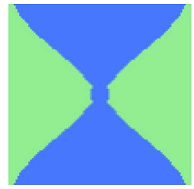	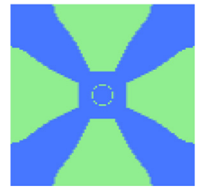	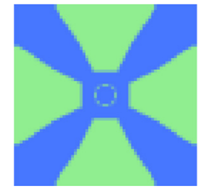
3 × 3 periodic arrangements	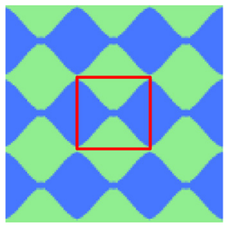	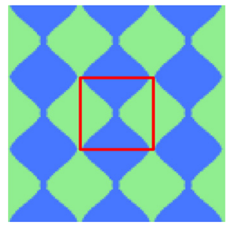	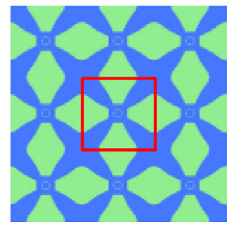	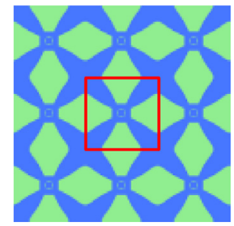
Equivalent elasticity matrix	$\begin{bmatrix} 1.0525 & 0.1716 & 0 \\ 0.1716 & 0.8570 & 0 \\ 0 & 0 & 0.1503 \end{bmatrix}$	$\begin{bmatrix} 0.8570 & 0.1716 & 0 \\ 0.1716 & 1.0525 & 0 \\ 0 & 0 & 0.1503 \end{bmatrix}$	$\begin{bmatrix} 0.9367 & 0.2086 & 0 \\ 0.2086 & 0.9367 & 0 \\ 0 & 0 & 0.1848 \end{bmatrix}$	$\begin{bmatrix} 0.8938 & 0.2395 & 0 \\ 0.2395 & 0.8938 & 0 \\ 0 & 0 & 0.2506 \end{bmatrix}$
Thermal conductivity matrix	$\begin{bmatrix} 1.7602 & 0 \\ 0 & 1.0884 \end{bmatrix}$	$\begin{bmatrix} 1.0884 & 0 \\ 0 & 1.7602 \end{bmatrix}$	$\begin{bmatrix} 1.6078 & 0 \\ 0 & 1.6078 \end{bmatrix}$	$\begin{bmatrix} 1.5245 & 0 \\ 0 & 1.5245 \end{bmatrix}$
Shear modulus	0.1503	0.1503	0.1848	0.2506
Conductivities	2.8486	2.8486	3.2156	3.0490
MH	0.5013	0.5013	0.4958	0.5786

Table 11
Optimized thermal insulation and shear modulus for hard A5.

Type	Case 5	Case 6	Case 7	Case 8
PUC	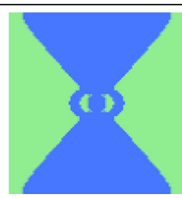	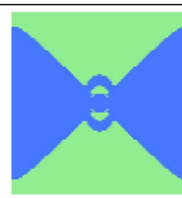	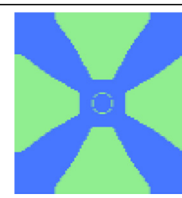	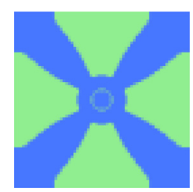
3 × 3 periodic arrangements	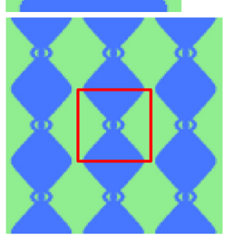	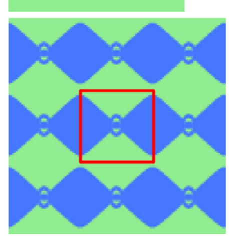	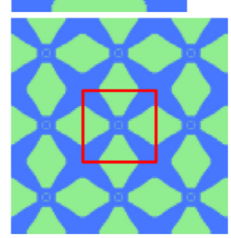	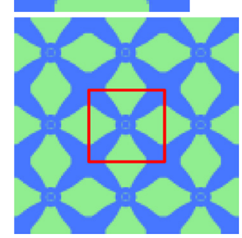
Equivalent elasticity matrix	$\begin{bmatrix} 1.0153 & 0.1707 & 0 \\ 0.1707 & 0.9141 & 0 \\ 0 & 0 & 0.1350 \end{bmatrix}$	$\begin{bmatrix} 0.9141 & 0.1707 & 0 \\ 0.1707 & 1.0153 & 0 \\ 0 & 0 & 0.1350 \end{bmatrix}$	$\begin{bmatrix} 0.9412 & 0.2116 & 0 \\ 0.2116 & 0.9412 & 0 \\ 0 & 0 & 0.1895 \end{bmatrix}$	$\begin{bmatrix} 0.8477 & 0.2558 & 0 \\ 0.2558 & 0.8477 & 0 \\ 0 & 0 & 0.2364 \end{bmatrix}$
Thermal conductivity matrix	$\begin{bmatrix} 1.4327 & 0 \\ 0 & 1.5696 \end{bmatrix}$	$\begin{bmatrix} 1.5696 & 0 \\ 0 & 1.4327 \end{bmatrix}$	$\begin{bmatrix} 1.6093 & 0 \\ 0 & 1.6093 \end{bmatrix}$	$\begin{bmatrix} 1.0429 & 0 \\ 0 & 1.0429 \end{bmatrix}$
Shear modulus	0.1350	0.1350	0.1895	0.2364
Conductivities	3.0022	3.0022	3.2186	3.1816
MH	0.4681	0.4681	0.5002	0.5507

shaped configurations except for the differences in the middle of the design domain, one is square and the other is round. The previous two cases possess the worst shear moduli, and the best insulation performances due to their maximum conductivities. Moreover, they have the lowest MH values of 0.4681. Case 7 has the middle shear modulus and the minimum insulation value, its MH value is the middle one. Case 8 possesses the best shear modulus and middle insulation value, leading to the best compound performance.

As depicted in Fig. 7, the curves related to objective functions and sub-objective functions are smooth enough, demonstrating that the proposed algorithm possesses good robustness to obtain hierarchical material microstructures, it is easy to find that the evolutionary histories in sub-objective function 2 are also stable during the optimization. Volume fractions in the two cases show the same changing trends, the evolutionary algorithm starts from a near-solid structure and gradually converge to the specified volume fractions of 0.5 in the 36th iteration. In addition, more than 10 iterations are needed to obtain the satisfactory accuracies. The topological evolutions are similar in different iterations and they finally converge to the same configurations, except for the differences in the central shapes of the design domain.

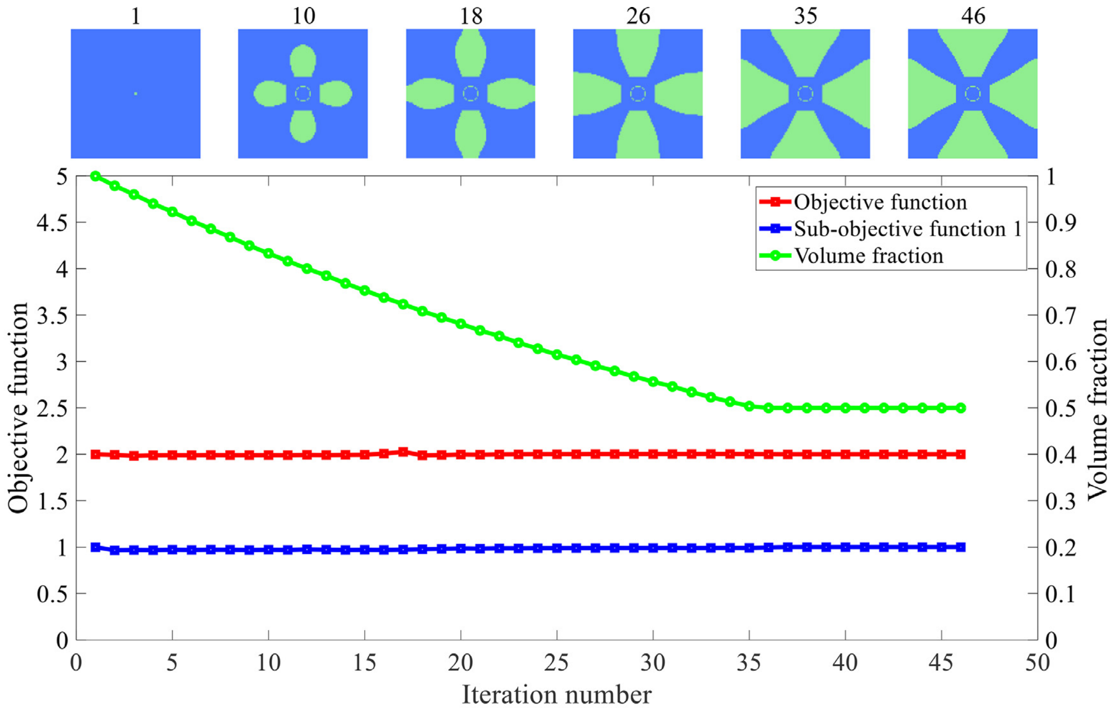

(a)

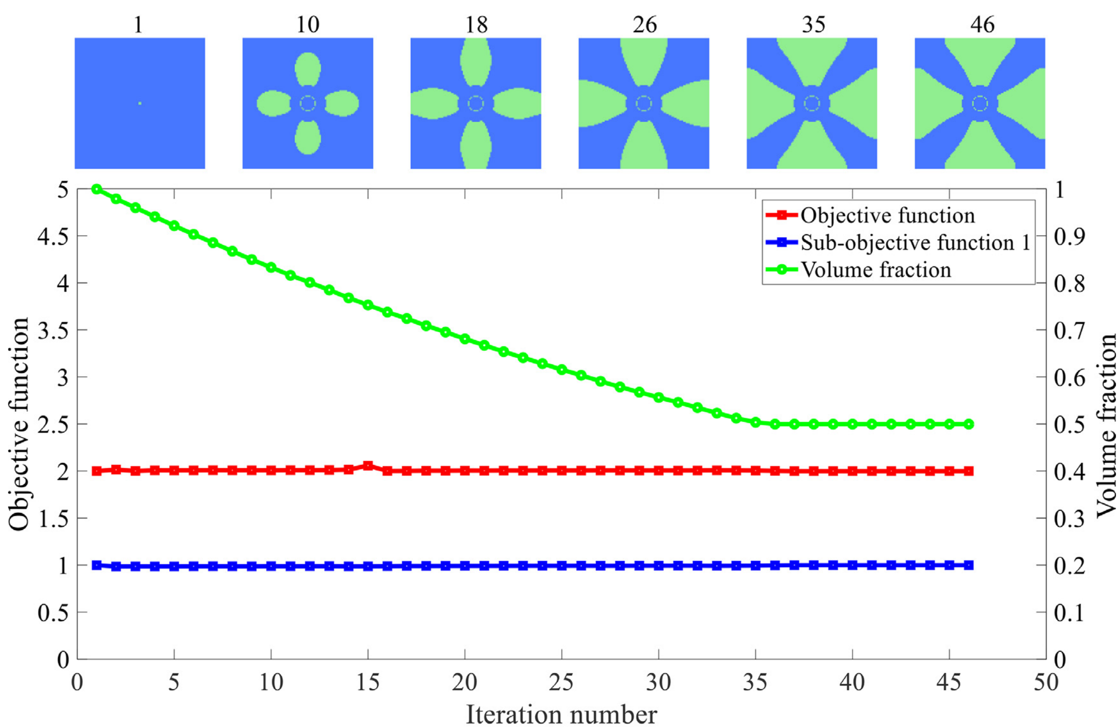

(b)

Fig. 7. Evolutionary histories of case 4 and case 8. (a) Soft A5; (b) hard A5.

5.4. Thermal insulation as well as bulk and shear moduli optimization

This example dedicates to obtain hierarchical material microstructures with thermal insulation and two moduli, accompanying by the compound performances in thermal insulation, bulk modulus and shear modulus simultaneously. As analyzed in the previous Sections, M1 material has the stronger performance in both the mechanics and thermal conductivities. In other words, M1 possesses better performance in mechanics but poor performance in thermal insulation. This example fixes the equivalent elasticity matrixes of M1 and M2 materials, and switches their thermal conductivities to illustrate how the opposite conductivities will influence the topological configurations of hierarchical materials. Here,

Table 12
M1 with strong mechanical performance and strong thermal conductivity.

Type	Case 1	Case 2	Case 3	Case 4
PUC			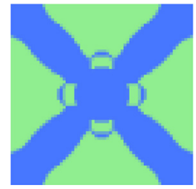	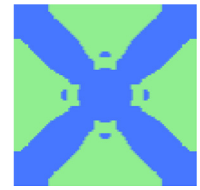
3 × 3 periodic arrangements	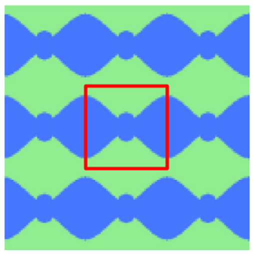	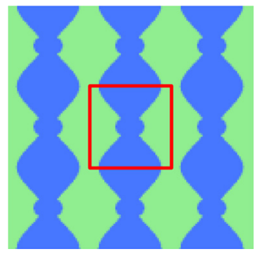	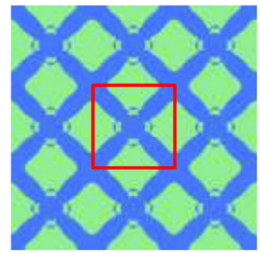	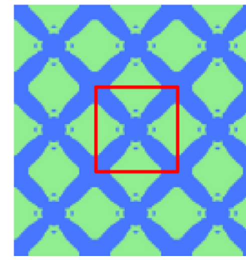
Equivalent elasticity matrix	$\begin{bmatrix} 3.6994 & 0.5404 & 0 \\ 0.5404 & 2.5683 & 0 \\ 0 & 0 & 0.4663 \end{bmatrix}$	$\begin{bmatrix} 2.5683 & 0.5404 & 0 \\ 0.5404 & 3.6994 & 0 \\ 0 & 0 & 0.4663 \end{bmatrix}$	$\begin{bmatrix} 2.9201 & 0.6893 & 0 \\ 0.6893 & 2.9201 & 0 \\ 0 & 0 & 0.6025 \end{bmatrix}$	$\begin{bmatrix} 2.8073 & 0.7866 & 0 \\ 0.7866 & 2.8073 & 0 \\ 0 & 0 & 0.8343 \end{bmatrix}$
Thermal conductivity matrix	$\begin{bmatrix} 4.1636 & 0 \\ 0 & 2.9096 \end{bmatrix}$	$\begin{bmatrix} 2.9096 & 0 \\ 0 & 4.1636 \end{bmatrix}$	$\begin{bmatrix} 3.7294 & 0 \\ 0 & 3.7294 \end{bmatrix}$	$\begin{bmatrix} 3.5512 & 0 \\ 0 & 3.5512 \end{bmatrix}$
two moduli	7.8149	7.8149	7.8215	8.0221
Conductivities	7.0732	7.0732	7.4589	7.1025
MH	7.9563	7.9563	7.9556	8.1629

Table 13
M1 with strong mechanical performance but weak thermal conductivity.

Type	Case 1	Case 2	Case 3	Case 4
PUC	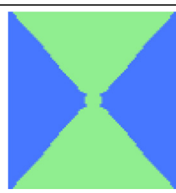	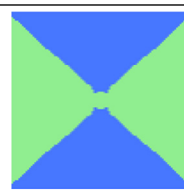	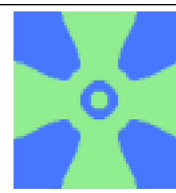	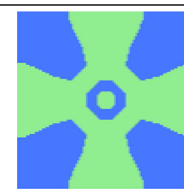
3 × 3 periodic arrangements	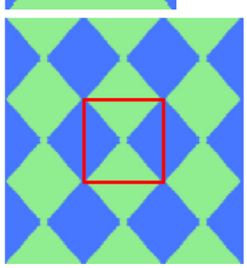	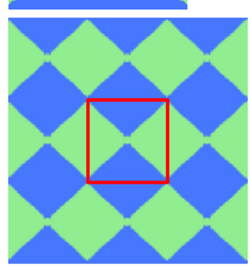	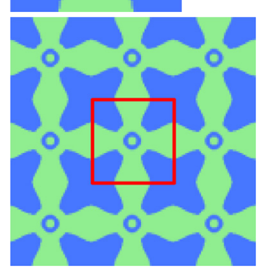	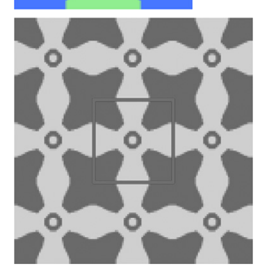
Equivalent elasticity matrix	$\begin{bmatrix} 3.1064 & 0.5242 & 0 \\ 0.5242 & 2.7628 & 0 \\ 0 & 0 & 0.4700 \end{bmatrix}$	$\begin{bmatrix} 2.7628 & 0.5242 & 0 \\ 0.5242 & 3.1064 & 0 \\ 0 & 0 & 0.4700 \end{bmatrix}$	$\begin{bmatrix} 2.9314 & 0.5750 & 0 \\ 0.5750 & 2.9314 & 0 \\ 0 & 0 & 0.5349 \end{bmatrix}$	$\begin{bmatrix} 2.7603 & 0.6633 & 0 \\ 0.6633 & 2.7603 & 0 \\ 0 & 0 & 0.6474 \end{bmatrix}$
Thermal conductivity matrix	$\begin{bmatrix} 4.9419 & 0 \\ 0 & 4.4200 \end{bmatrix}$	$\begin{bmatrix} 4.4200 & 0 \\ 0 & 4.9419 \end{bmatrix}$	$\begin{bmatrix} 5.0190 & 0 \\ 0 & 5.0190 \end{bmatrix}$	$\begin{bmatrix} 5.0693 & 0 \\ 0 & 5.0693 \end{bmatrix}$
Two moduli	7.3876	7.3876	7.5477	7.4946
Conductivities	9.3619	9.3619	10.0380	10.1387
MH	7.4944	7.4944	7.6473	7.5932

case 1∼4 are utilized to analysis without consideration of case 5∼8. The elastic moduli and thermal conductivities of the two base materials to make up M1 and M2 are set to 10 and 3, respectively. Table 12 lists all the calculation results under M1 with strong mechanical performance and strong thermal conductivity, Table 13 lists all the calculation results under M1 with strong mechanical performance but weak thermal conductivity. Obviously, the thermal conductivities of the two base materials in Table 12 are 10 and 3, but the two values are opposite in Table 13.

As listed in Table 12, case 1 and case 2 exhibit the dumbbell-shaped configurations in the x- and y-directions, respectively, case 3 and case 4 show the fan-shaped configurations, respectively. The topological results are similar to the cases analyzed in Sections 5.2 and 5.3, which demonstrates that the compound performances of hierarchical materials in mechanics and thermal insulation are roughly the same, because those microstructures with good bulk modulus usually have good shear modulus at the same time, and vice versa. Although case 1 and case 2 have the min-

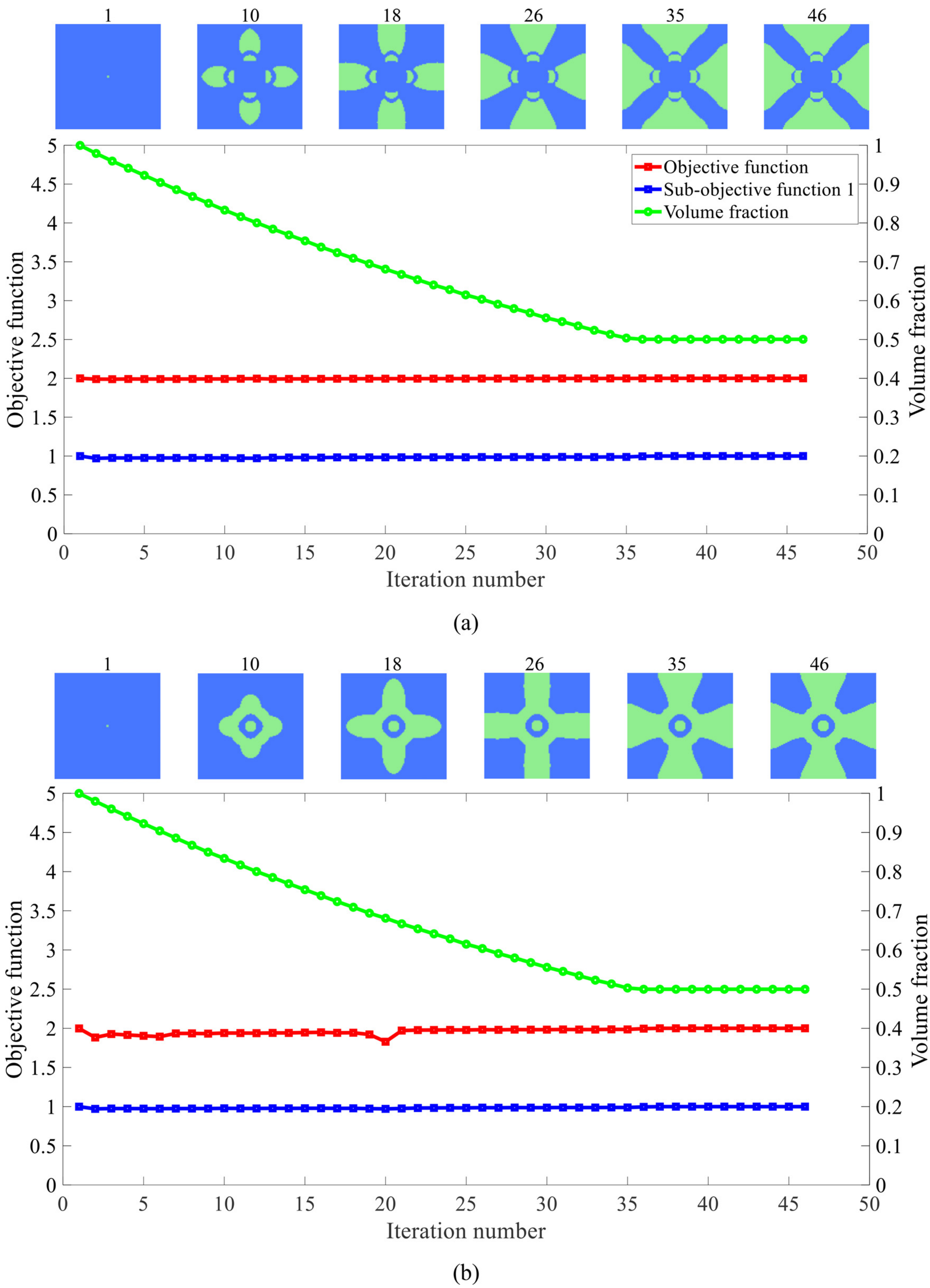

Fig. 8. Evolutionary histories of case 3 under different conductivities in M1. (a) Strong conductivity in M1; (b) weak conductivity in M1.

imum moduli and conductivities, their MHs are the middle ones, which has a little advantage over case 3. Case 3 has the best conductivity and middle moduli, and its MH value is the worst one. Case 4 possesses the maximum moduli and middle conductivity, it shows the best compound performance. Furthermore, the compound performances of the obtained hierarchical materials have nothing to do with the magnitude orders of their respective moduli and conductivities.

As listed in Table 13, when the thermal conductivities in M1 and M2 are exchanged, case 1∼4 show completely different topologies when compared to those results listed in Table 12. M2 material connects well in all cases, but M1 is separated to insulate the heat transmissions due to its lower thermal conductivity. Case 1 and case 2 possess the minimum moduli and conductivities, and their MHs are also the smallest ones. Case 3 possesses the maximum modulus and middle conductivity, it performs the best composite performance because of the maximum MH. Case 4 has the middle modulus and the worst insulation, and its MH value of 7.5932 is the middle one. Table 13 further demonstrates that the compound performances of hierarchical material microstructures are consistent with the magnitude sequence of their mechanical moduli in most cases, rather than their conductivities.

As depicted in Fig. 8, all curves are extremely smooth. In Fig. 8(b), there is a little shock at the 20th iteration, which may correspond to a violent stage of topological evolution. After that, the objective function is stable around 2 until the optimization ends. The curves related to sub-objective function 1 is smooth enough, it is easy to find that sub-objective function 2 should has the same oscillation as the total objective function. Volume fractions gradually converge to the specified value of 0.5, which reflects the unique advantage of evolutionary algorithm. Topological evolutions are basically stable during the optimization.

6. Conclusions

This study proposes a new design methodology to create hierarchical material microstructures with two phases, which are composed of porous base materials. To achieve different multifunctional designs, such as thermal insulation with bulk modulus, thermal insulation with shear modulus and thermal insulation with two moduli, an adaptive weight coefficient adjusting method is presented to approach the Pareto frontiers, regardless of the number of the individual objective functions. The fast convergence of the design (all examples converged within 50 iterations) demonstrates the efficiency of the evolutionary method. Hierarchical design results for the single performance and multiple performances are very different, cases related to A1 and A2 configurations always show the same performances, despite the difference of the obtained topological configurations of material microstructures. Cases related to A3 and A4 configurations exhibit the similar topologies but different properties. The following conclusions can be drawn:

(1) For the design of single performance, case 1 and case 2 related to A1 and A2 configurations show the best bulk moduli, case 4 related to A4 configuration is the worst one, but the magnitude order of cases 1∼4 in the shear modulus is reversed. Case 4 has the best performance in thermal insulation, whereas case 3 related to A3 configuration shows the worst insulation.
(2) For the design of thermal insulation with bulk modulus, cases related to A1 and A2 configurations show the worst composite performances. Case 4 shows the best compound performance in the previous four cases, but case 7 related to A3 configuration is the best one among cases 5∼8.
(3) For the design of thermal insulation with shear modulus, cases related to A4 configuration have the superior compound performances than others. Case 3 shows the worst composite performance in the previous four cases, but case 5 and case 6 related to A1 and A2 configurations are the worst ones among cases 5∼8.
(4) For the design of thermal insulation with two moduli, cases related to A1 and A2 configurations show the worst compound performances. Case 4 shows the best composite performance in the previous four cases, but case 3 performs the best when the conductivities of the two PBMs are exchanged.

The above conclusions explain that both the exchanges of two PBMs and conductivities will impact the design of hierarchical materials. The proposed method is featured with high efficiency, easiness in implementation, good connectivity and clear interface between adjacent phases. Although the proposed method is tested on the 2D numerical examples, it can be applied to 3D designs without any conceptual difficulties. Moreover, our future work will focus on the experimental verification of the multiple performances in both the mechanics and thermal insulation.

Author statements

Yongfeng Zheng: Methodology, programming, writing and editing; **Zhuojia Fu:** Check and discussion; **Yingjun Wang:** Drawing and conceptualization; **Xiang Lu:** Check and discussion; **Jinping Qu:** Supervision and review; **Chuanzeng Zhang:** Supervision, review and revise.

Declaration of Competing Interest

The authors declare that they have no known competing financial interests or personal relationships that could appeared to influence the work reported in this paper.

Acknowledgments

This research is supported by the Guangdong Basic and Applied Basic Research Foundation (grant no. 2019A1515110183), the Postdoctoral Research Foundation of China (grant no. 2020M682699), and the Opening Project of Guangdong Provincial Key Laboratory of Technique and Equipment for Macromolecular Advanced Manufacturing, South China University of Technology, China (grant no. 2021kfkt04). Moreover, the first author would like to thank the China Scholarship Council (CSC) and the Germany Academic Exchange Service (DAAD) to jointly support his Postdoctoral Fellowship at the Chair of Structural Mechanics, University of Siegen, Germany.

References

[1] Q. Xi, Z. Fu, T. Rabczuk, An efficient boundary collocation scheme for transient thermal analysis in large-size-ratio functionally graded materials under heat source load, Comput. Mech. (2019).
[2] Z. Fu, Q. Xi, W. Chen, A.H.-.D. Cheng, A boundary-type meshless solver for transient heat conduction analysis of slender functionally graded materials with exponential variations, Comput. Math. Appl. 76 (2018) 760–773.
[3] Z. Fu, L. Yang, Q. Xi, C. Liu, A boundary collocation method for anomalous heat conduction analysis in functionally graded materials, Comput. Math. Appl. 88 (2021) 91–109.
[4] J. Guo, Z. Qu, X. Wang, A reverse thermal cloak design method based on inverse problem theory, ES Energy Environ. 7 (2020) 71–83.
[5] Y. Xiao, Q. Chen, Q Hao, Inverse thermal design of nanoporous thin films for thermal cloaking, Mater. Today Phys. 21 (2021) 100477.
[6] L. Sun, L. Liang, Z. Shi, H. Wang, R Fan, Optimizing strategy for the dielectric performance of topological-structured polymer nanocomposites by rationally tailoring the spatial distribution of nanofillers, Eng. Sci. 12 (2020) 95–105.
[7] M. Bendsøe, O. Sigmund, Topology Optimization: Theory, Method and Applications, Springer, 2003.
[8] L. Xia, Q. Xia, X. Huang, Y.M. Xie, Bi-directional evolutionary structural optimization on advanced structures and materials: a comprehensive review, Arch. Comput. Meth. Eng. 25 (2016) 437–478.
[9] M. Bendsøe, N. Kikuchi, Generating optimal topologies in structural design using a homogenization method, Comput. Method. Appl. Mech. Eng. 71 (1988) 197–224.
[10] Y.M. Xie, G.P. Steven, A simple evolutionary procedure for structural optimization, Comput. Struct. 49 (1993) 885–896.
[11] C.G. Zhuang, Z.H. Xiong, H. Ding, Temperature-constrained topology optimization of nonlinear heat conduction problems, J. Comput. Des. Eng. 8 (2021) 1059–1081.
[12] Z. Luo, N. Zhang, Y. Wang, W. Gao, Topology optimization of structures using meshless density variable approximants, Int. J. Numer. Methods Eng. 93 (2013) 443–464.
[13] Y. Wang, Z. Liao, M. Ye, Y. Zhang, W. Li, Z. Xia, An efficient isogeometric topology optimization using multilevel mesh, MGCG and local-update strategy, Adv. Eng. Softw. 139 (2020) 102733.
[14] X. Huang, Smooth topological design of structures using the floating projection, Eng. Struct. 208 (2020) 110330.
[15] M.Y. Wang, X. Wang, D. Guo, A level set method for structural topology optimization, Comput. Method. Appl. Mech. Eng. 192 (2003) 227–246.

[16] G. Allaire, F. Jouve, A. Toader, Structural optimization using sensitivity analysis and a level-set method, J. Comput. Phys. 194 (2004) 363–393.
[17] Z. Luo, M.Y. Wang, S. Wang, P Wei, A level set-based parameterization method for structural shape and topology optimization, Int. J. Numer. Methods Eng. 76 (2010) 1–26.
[18] A.L. Gain, G.H. Paulino, Phase-field based topology optimization with polygonal elements: a finite volume approach for the evolution equation, Struct. Multidiscipl. Optim. 46 (2012) 327–342.
[19] L. Dedè, M.J. Borden, T.J.R. Hughes, Isogeometric analysis for topology optimization with a phase field model, Arch. Comput. Meth. Eng. 19 (2012) 427–465.
[20] X Guo, A 188-line matlab code for Moving Morphable Component (MMC) method for topology optimization, Struct. Multidiscipl. Optim. (2015).
[21] Y. Wang, D.J. Benson, Isogeometric analysis for parameterized LSM-based structural topology optimization, Comput. Mech. 57 (2016) 19–35.
[22] Q. Xia, T. Shi, L. Xia, Topology optimization for heat conduction by combining level set method and BESO method, Int. J. Heat Mass Transf. 127 (2018) 200–209.
[23] X. Huang, Y.M. Xie, Convergent and mesh-independent solutions for the bi-directional evolutionary structural optimization method, Finite Element. Analy. Des. 43 (2007) 1039–1049.
[24] O. Sigmund, Tailoring materials with prescribed elastic properties, Mech. Mater. 20 (1995) 351–368.
[25] S. Zhou, J. Cadman, Y. Chen, L. Wei, M.X. Yi, X. Huang, et al., Design and fabrication of biphasic cellular materials with transport properties - A modified bidirectional evolutionary structural optimization procedure and MATLAB program, Int. J. Heat Mass Transf. 55 (2012) 8149–8162.
[26] S. Zhou, Q. Li, Computational design of multi-phase microstructural materials for extremal conductivity, Comput. Mater. Sci. 43 (2008) 549–564.
[27] Y. Wang, Z. Luo, N. Zhang, Z. Kang, Topological shape optimization of microstructural metamaterials using a level set method, Comput. Mater. Sci. 87 (2014) 178–186.
[28] J. Wu, Z. Luo, H. Li, N. Zhang, Level-set topology optimization for mechanical metamaterials under hybrid uncertainties, Comput. Method. Appl. Mech. Eng. 319 (2017) 414–441.
[29] Y. Wang, J. Gao, Z. Luo, T. Brown, N. Zhang, Level-set topology optimization for multimaterial and multifunctional mechanical metamaterials, Eng. Optim. 49 (2017) 22–42.
[30] Y. Wang, H. Xu, D. Pasini, Multiscale isogeometric topology optimization for lattice materials, Comput. Method. Appl. Mech. Eng. 316 (2017) 568–585.
[31] J. Gao, H. Xue, L. Gao, Z. Luo, Topology optimization for auxetic metamaterials based on isogeometric analysis, Comput. Method. Appl. Mech. Eng. 352 (2019) 211–236.
[32] J. Xu, L. Gao, M. Xiao, J. Gao, H Li, Isogeometric topology optimization for rational design of ultra-lightweight architected materials, Int. J. Mech. Sci. 166 (2020) 105103.
[33] X. Yan, X. Huang, G. Sun, Y.M. Xie, Two-scale optimal design of structures with thermal insulation materials, Compos. Struct. 120 (2015) 358–365.
[34] A. Radman, X. Huang, Y.M. Xie, Topological design of microstructures of multi-phase materials for maximum stiffness or thermal conductivity, Comput. Mater. Sci. 91 (2014) 266–273.
[35] X. Huang, Y.M. Xie, B. Jia, Q. Li, S.W. Zhou, Evolutionary topology optimization of periodic composites for extremal magnetic permeability and electrical permittivity, Struct. Multidiscip. Optim. 46 (2012) 385–398.
[36] L.G. Page, J. Dirker, J.P. Meyer, Topology optimization for the conduction cooling of a heat-generating volume with orthotropic material, Int. J. Heat Mass Transf. 103 (2016) 1075–1083.
[37] R. Alberdi, K. Khandelwal, Bi-material topology optimization for energy dissipation with inertia and material rate effects under finite deformations, Finite Elem. Anal. Des. 164 (2019) 18–41.
[38] K.M. Hamdia, H. Ghasemi, Y. Bazi, H. Alhichri, N. Alajlan, T. Rabczuk, A novel deep learning based method for the computational material design of flexoelectric nanostructures with topology optimization, Finite Elem. Anal. Des. 165 (2019) 21–30.
[39] M. Ye, L. Gao, H. Li, A design framework for gradually stiffer mechanical metamaterial induced by negative Poisson's ratio property, Mater. Des. 192 (2020) 108751.
[40] H. Li, Z. Luo, L. Gao, Q. Qin, Topology optimization for concurrent design of structures with multi-patch microstructures by level sets, Comput. Method. Appl. Mech. Eng. 331 (2018) 536–561.
[41] Z. Li, Z. Luo, L.C. Zhang, C.H. Wang, Topological design of pentamode lattice metamaterials using a ground structure method, Mater. Des. (2021) 109523.
[42] S. Wu, Z. Luo, Z. Li, S. Liu, L.-C. Zhang, Topological design of pentamode metamaterials with additive manufacturing, Comput. Method. Appl. Mech. Eng. 377 (2021) 113708.
[43] Y. Zheng, Y. Wang, X. Lu, Z. Liao, J. Qu, Evolutionary topology optimization for mechanical metamaterials with auxetic property, Int. J. Mech. Sci. 179 (2020) 105638.
[44] Y. Zheng, Y. Wang, X. Lu, J. Zheng, J. Qu, Topology optimisation for isotropic mechanical metamaterials considering material uncertainties, Mech. Mater. (2021) 103742.
[45] Y. Zheng, Y. Wang, Z. Luo, X. Lu, J. Qu, Concurrent design for structures and material microstructures under hybrid uncertainties, Mater. Des. (2021) 109728.
[46] X. Zhang, J. Xing, P. Liu, Y. Luo, Z. Kang, Realization of full and directional band gap design by non-gradient topology optimization in acoustic metamaterials, Extreme Mech. Lett. 42 (2021) 101126.
[47] L. Ai, X.L Gao, Metamaterials with negative Poisson's ratio and non-positive thermal expansion, Compos. Struct. 162 (2017) 70–84.
[48] H. Deng, S. Hinnebusch, A.C. To, Topology optimization design of stretchable metamaterials with Bézier skeleton explicit density (BSED) representation algorithm, Comput. Method. Appl. Mech. Eng. 366 (2020) 113093.
[49] L. Alacoque, R.T. Watkins, A.Y. Tamijani, Stress-based and robust topology optimization for thermoelastic multi-material periodic microstructures, Comput. Method. Appl. Mech. Eng. 379 (2021) 113749.
[50] R. Xu, J. Yang, W. Yan, Q. Huang, H. Hu, Data-driven multiscale finite element method: from concurrence to separation, Comput. Method. Appl. Mech. Eng. 363 (2020) 112893.
[51] Q. Shao, J. Liu, Q. Huang, J. Yang, H. Hu, S. Belouettar, et al., A data-driven analysis on bridging techniques for heterogeneous materials and structures, Mech. Adv. Mater. Struct. (2019) 1–15.
[52] W.M. Vicente, Z.H. Zuo, R. Pavanello, T. Calixto, R. Picelli, Y.M. Xie, Concurrent topology optimization for minimizing frequency responses of two-level hierarchical structures, Comput. Method. Appl. Mech. Eng. 301 (2016) 116–136.
[53] J. Gao, Z. Luo, H. Li, P. Li, L. Gao, Dynamic multiscale topology optimization for multi-regional micro-structured cellular composites, Compos. Struct. 211 (2019) 401–417.
[54] G. Marck, M. Nemer, J.-L. Harion, S. Russeil, D. Bougeard, Topology optimization using the SIMP method for multiobjective conductive problems, Num. Heat Transf. Part B 61 (2012) 439–470.
[55] N.D. Kruijf, S. Zhou, Q. Li, Y.W Mai, Topological design of structures and composite materials with multiobjectives, Int. J. Solids Struct. 44 (2007) 7092–7109.
[56] E. Andreassen, C.S. Andreasen, How to determine composite material properties using numerical homogenization, Comput. Mater. Sci. 83 (2014) 488–495.
[57] L. Xia, P. Breitkopf, Design of materials using topology optimization and energy-based homogenization approach in Matlab, Struct. Multidiscipl. Optim. 52 (2015) 1229–1241.
[58] H. Li, L. Gao, H. Li, H. Tong, Spatial-varying multi-phase infill design using density-based topology optimization, Comput. Method. Appl. Mech. Eng. 372 (2020) 113354.
[59] M.P. Bendsøe, O. Sigmund, Material interpolation schemes in topology optimization, Arch. Appl. Mech. 69 (1999) 635–654.
[60] Y. Xiao, Q. Hao, Nanoslot patterns for enhanced thermal anisotropy of Si thin films, Int. J. Heat Mass Transf. 170 (2021) 120944.
[61] D.C. Da, X.Y. Cui, K. Long, G.Y. Li, Concurrent topological design of composite structures and the underlying multi-phase materials, Comput. Struct. 179 (2017) 1–14.
[62] O. Sigmund, A 99 line topology optimization code written in Matlab, Struct. Multidiscipl. Optim. 21 (2001) 120–127.